analytical chemistry

pubs.acs.org/ac Review

Instrumentation for Hydrogenative Parahydrogen-Based Hyperpolarization Techniques

Andreas B. Schmidt,* C. Russell Bowers, Kai Buckenmaier, Eduard Y. Chekmenev, Henri de Maissin, James Eills, Frowin Ellermann, Stefan Glöggler, Jeremy W. Gordon, Stephan Knecht, Igor V. Koptyug, Jule Kuhn, Andrey N. Pravdivtsev, Francesca Reineri, Thomas Theis, Kolja Them, and Jan-Bernd Hövener*

Cite This: *Anal. Chem.* 2022, 94, 479−502

CONTENTS

The unique properties of the entangled, antisymmetric nuclear spin state of dihydrogen, parahydrogen (pH_2), has intrigued physicists, chemists, and other scientists for almost a century. pH_2 was used as a model system in the early days of quantum mechanics[1] and is used for fueling rockets as well as combustion-free cars today. In the 1980s, pH_2 was discovered as a convenient and potent source of spin order, allowing the enhancement of the signals of magnetic resonance (MR) by several orders of magnitude.[2−4] In the advent of hyperpolarized (HP) contrast agents (CA) for biomedical MR imaging (MRI) that followed, pH_2-based hyperpolarization methods played an important role in the acquisition of the first HP ^{13}C *in vivo* images (Figure 1).[5,6] Ever since, pH_2 has proven to be highly valuable for analytical investigations and fundamental research, *e.g.*, in analytical and catalytic chemistry or in the physics of singlet spin states.[7−10]

pH_2 can be produced rapidly and stored easily. As one of four (nuclear) spin states of dihydrogen, 25% of H_2 at room temperature is pH_2, while the other 75% is orthohydrogen (oH_2), following the Boltzmann distribution). At lower temperatures, however, the *para*-fraction increases until at approximately 25 K, where 100% pH_2 is obtained. While the *para*-enrichment is fast using an appropriate catalyst, pH_2 can be stored for hours to days at room temperature without significant loss if the catalyst is absent. These unique properties make pH_2 an ideal host of pure spin order that can be produced easily, stored conveniently (in a pressurized bottle),

Special Issue: Fundamental and Applied Reviews in Analytical Chemistry 2022

Published: January 1, 2022

https://doi.org/10.1021/acs.analchem.1c04863
Anal. Chem. 2022, 94, 479−502

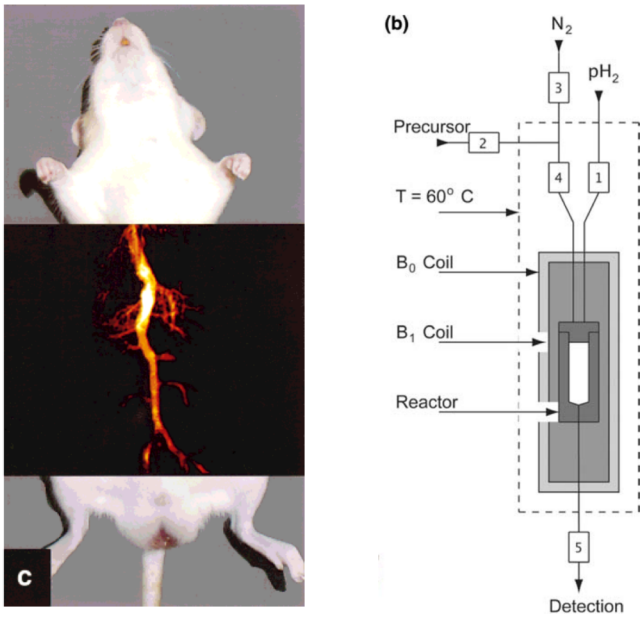

Figure 1. First hyperpolarized ^{13}C *in vivo* MRI ever published (a). The contrast agent, hydroxyethyl [1-^{13}C]propionate-d_3 (HEP), was produced using a prototype commercial PHIP polarizer (Amersham Biosciences, healthcare company), similar to the one shown schematically in (b). Broadly speaking, the polarizers consisted of a unit handling the fluids, the actual hyperpolarization (spin-order transfer), and the coordination of the entire process (numbers 1−5 represent valves). Images reproduced from Parahydrogen-Induced Polarization in Imaging: Subsecond ^{13}C Angiography, Golman, K.; Axelsson, O.; Johannesson, H.; Mansson, S.; Olofsson, C.; Petersson, J. S. *Magn. Reson. Med.*, Vol. *46*, Issue 1, 1−5 (ref 5). Copyright 2001 Wiley (a) and reprinted by permission from Springer: *Magn. Reson. Mater. Phys.*, PASADENA Hyperpolarization of ^{13}C Biomolecules: Equipment Design and Installation, Hövener, J.-B.; Chekmenev, E. Y.; Harris, K. C.; Perman, W. H.; Robertson, L. W.; Ross, B. D.; Bhattacharya, P. *Magn. Reson. Mater. Phys.* Vol. 22, 111−121 (ref 90). Copyright Springer 2009 (b).

and used on demand, *e.g.*, for producing hyperpolarized CAs or observing chemical reactions with enhanced sensitivity.

When it comes to clinical applications, however, dissolution dynamic nuclear polarization (dDNP) evolved faster than pH_2-based HP methods.[11,12] The reasons for this may be that (a) at first, only a few biologically relevant CAs were available (because of limited chemistry at that time), (b) that mastering the complex process of parahydrogen induced polarization (PHIP) was not straightforward (involving quantum mechanics, chemical reactions, and magnetic resonance methods tailored to each individual CA), and that (c) no pH_2-polarizers were commercially available, while there were at least three different dDNP polarizer generations.

While pH_2 is easily produced in large quantities, at low cost and with a shelf life of days (depending on the storing conditions), there are some hurdles to overcome before a CA is ready for administration. For one, the pH_2 spin order *per se* is MR invisible (total spin of 0!) and well hidden inside the dihydrogen molecule. To obtain a hyperpolarized CA from pH_2, typically, the following steps have to be taken: (a) to bring pH_2 and the target into contact (by catalytic addition or reversible exchange), (b) to transfer or transform the pH_2-derived spin order into a desired form, and (c) the purification and quality assurance (QA) prior to an *in vivo* application.

These steps usually involve a chemical reaction at elevated temperatures, pressures, sometimes in aggressive media or extreme pH, synchronized with quantum mechanical spin order transfer (SOT) mediated by evolution at constant or varying magnetic fields and radiofrequency (RF) pulses. To realize this process, various devices have been devised; however, a single, unified design has not yet emerged. The lack of such a device may be attributed to the fact that the power and versatility of pH_2 has resulted in quite a few different methods; the magnetic fields alone vary by a factor of 10^9 (from nanotesla to tesla). Even today, pH_2 hyperpolarization methods keep evolving at a fast pace; among the ground-breaking advances, SABRE,[13] gases,[14,15] continuous HP,[16−18] PHIP-SAH,[19] RASER,[20−23] purification methods,[24] and relay methods[25,26] are only a few examples from the past decade. These methods require specific experimental conditions and ultimately dedicated instrumentation, which differs from method to method.

For a standardized, clinical application of a specific contrast agent, however, a consolidated setup is required that can be certified and approved and provides reliable polarization and quality assurance. In this respect, much can be learned from SEOP[27] and DNP[11,12] with respect to polarizers and regulatory approval.

Here, we review the different instrumentations for pH_2 hyperpolarization, with an emphasis on biomedical applications. To keep this review concise, we focus on setups for hydrogenative pH_2-based hyperpolarization alone and the most recent literature (~last 5 years); still, we refer to pioneering and game-changing developments whenever appropriate and when other methods (SABRE, DNP, SEOP, etc.) show similar instrumentational aspects. Dedicated reviews on SABRE-related instrumentation, spin-order transfer, and pH_2 production are expected to be published elsewhere.

■ ANALYSIS OF pH_2 POLARIZERS

The requirements for a biomedical polarizer may be defined as to (i) provide a clean, (ii) aqueous solution of (iii) highly polarized, (iv) appropriately concentrated agents at (v) physiological conditions that is preferably produced in a (iv) good-manufacturing process (GMP). To make such a contrast agent, the role of hardware may be categorized as follows:

1. Making the pH_2 spin order available to the target molecule (hydrogenation);
2. Transferring the pH_2-derived spin order into the desired spin hyperpolarization (typically longitudinal X-nuclear magnetization);
3. Purification of the solution and assuring quality.

We will elaborate on these steps in the following.

Parahydrogen Addition. Before the addition, the lifetime of gaseous[28−30] or dissolved[31−33] pH_2 is typically long (days or many minutes, respectively). However, once bound to the catalyst[34] or the precursor,[9,35−39] the lifetime of the spin order is drastically reduced because the added protons, referred to as I_1 and I_2, interact with the environment and the rest of the (now larger) spin system. Thus, the hydrogenation should be conducted as fast as possible to reduce relaxation losses. The hydrogenation kinetics are typically affected by a multitude of coupled reaction parameters, like temperature, pH_2-availability, solvent, catalyst, precursor molecule, and pH. While the catalyst is needed for the addition, it may cause relaxation at

https://doi.org/10.1021/acs.analchem.1c04863
Anal. Chem. 2022, 94, 479−502

the same time and needs to be removed before an injection if it is harmful.

The starting point for the SOT, *i.e.*, the density matrix after the hydrogenation, is strongly dependent on the coupling between I_1 and I_2. It is determined by the molecular structure and the external static magnetic field B_0. If the spins are "strongly coupled" (that is, if their mutual J-coupling J_{12} is much larger than the difference of their Larmor precession frequencies $\delta\nu$ ($\delta\nu \ll J_{12}$)), the eigenstates of the two-spin system are essentially the singlet-triplet (S-T) basis states. In this case, the "singlet spin order" $\mathbf{I_1 \bullet I_2} = I_{1x}I_{2x} + I_{1y}I_{2y} + I_{1z}I_{2z}$ (also known as the J-order) is usually the starting point for the SOT. In the opposite case ($\delta\nu \gg J_{12}$), the spins are referred to as weakly coupled. Then, the $I_{1z}I_{2z}$ spin order is typically the starting point for SOT after the off-diagonal elements of the density matrix were averaged away during the hydrogenation.[40] However, the $\mathbf{I_1 \bullet I_2}$ order can be preserved in weakly coupled systems by applying sufficiently strong ^{1}H decoupling[41,42] or can be encountered in effectively instantaneous reactions as in photo-PHIP experiments,[43,44] where reactions with pH_2 happen within a few microseconds.

The exact form of the spin order in the intermediate coupling regime, including the effect from singlet-triplet (S-T) mixing at the hydrogenation catalysts, was described by Bowers, Natterer, and others.[39,45−48] Such S-T mixing takes place in high and low fields and is one of the main reasons for reduced hyperpolarization yield.

In so-called PASADENA experiments (pH_2 and synthesis allows dramatically enhanced nuclear alignment), hydrogenation and SOT (or direct proton detection) take place at the same magnetic field.[3] Another experimental scheme often applied is referred to as adiabatic longitudinal transport after dissociation engenders net alignment (ALTADENA).[49] The latter typically features hydrogenation at lower fields (with S-T eigenbasis) followed by an adiabatic (slow) increase of B_0 into the weakly coupled regime.[50] This results in population of either the $|\alpha\beta\rangle$ or the $|\beta\alpha\rangle$ state of the high-field Zeeman eigenbasis, where α is the spin up, and β is the spin down state in the combined spin angular momentum state of both nuclei.

Spin-Order Transfer. As the literature on SOT may fill an entire review article alone,[51] we are focusing on the parts relevant for the instrumentation only. The available spin order after hydrogenation, the spin system, its eigenstates, and its interactions determine the most-effective SOT strategy. While the molecular spin system as such is usually fixed (with workarounds, *e.g.*, PHIP-SAH,[19] PHIP-X[26]), the interactions can be tailored to some extent by varying the (static) external magnetic field (B_{SOT}) or by applying B_1 fields over a period of time.[52] Likewise, the spin system can be affected, to some degree, by isotope labeling and reaction parameters such as temperature and pH. Deuteration is a convenient way to reduce relaxation and simplify the spin system, *e.g.*, to an effective 3-spin-1/2 system in RF-pulsed SOT.[42,53,54]

Roughly speaking, a SOT can be achieved by

- Evolution at one static field (sometimes referred to as "spontaneous" transfer);
- Evolution at different fields, magnetic field cycling (MFC-SOT);[19,24,55,56]
- Evolution plus specific manipulations by RF pulses (RF-SOT).[9,40,42,51,57−64]

Understanding the SOT requires profound knowledge of the underlying quantum mechanics. While analytical equations can be derived for simple systems, numerical simulations are usually required to determine the optimal parameters of more complex or realistic systems. These simulations can be implemented in any programming environment capable of matrix algebra. Using or building on existing (open source) packages may be convenient.[65−68]

Realizing the different variants of SOT usually requires a magnet (superconducting, resistive, permanent; sometimes shims), sometimes a multilayer mu-metal shield (to reach fields B_{SOT} in the nanotesla or microtesla range), and an NMR unit to excite and receive MR signals.

Purification and Quality Assurance. While the addition of pH_2 is performed by catalysis at sometimes harsh conditions, a physiological solution devoid of the catalyst is needed for *in vivo* administration. Various approaches have been described to achieve this goal, including:

- Filtering homogeneous catalysts,[69]
- Using immobilized catalysts that remain in the polarizer,[70−72]
- Heterogeneous catalysts that facilitate filtration;[17,71,73−78]
- Phase separation and precipitation.[24,79−82]

Different agents will generally require individual approaches as their chemical properties vary significantly. A QA module similar to that used for DNP will have to encompass (at least) purity, pH, a low bioburden, and temperature; no such device has emerged yet. For all approaches, time is of the essence, as precious signal enhancement is rapidly lost once the agent is hyperpolarized.

Components and Capabilities of a Polarizer. Orchestrating these steps requires a dedicated unit, often referred to as a "polarizer". Some have been described, with varying goals, properties, and capabilities, *e.g.*, SOT schemes, pressures, temperatures, *in situ* detection, automation, dosing, etc.[24,36,38,42,55,83−91] For convenience, such a polarizer may be separated in different units, some of which were described in literature:

- A fluid unit, handling the gases and liquids. It is typically composed of electromagnetic, manual, or pneumatic valves and tubes, borrowed, *e.g.*, from high-performance liquid chromatography (HPLC) as well as a custom-made reaction chamber or a (high-pressure) NMR tube. Inert materials and pressure and temperature resistance are important factors, as is the option to clean or sterilize.[92]
- An NMR unit, taking care of the SOT either by applying a constant magnetic field, a defined field cycle, or RF pulses. Low-field detection facilitates flip angle calibration and quality assurance.[92−94]
- A control unit: a software controlling a digital-to-analog converter (DAC) and an analog-to-digital converter (ADC), *e.g.*, for switching valves, B_0 control, temperature readings, and NMR. These needs have been addressed by using the hardware of the NMR/MRI,[87,88,95] by PC-controlled digital-acquisition boards (DAQ) with[85,86] and without[42,55,83,89,90,96] an additional NMR spectrometer. As a minimum, the control software will have to accommodate easy access to the (sometimes overlapping) timings of each step in the polarization procedure and may extend to acquiring NMR signal *in situ* to facilitate calibrations and improve polarization

https://doi.org/10.1021/acs.analchem.1c04863
Anal. Chem. 2022, 94, 479−502

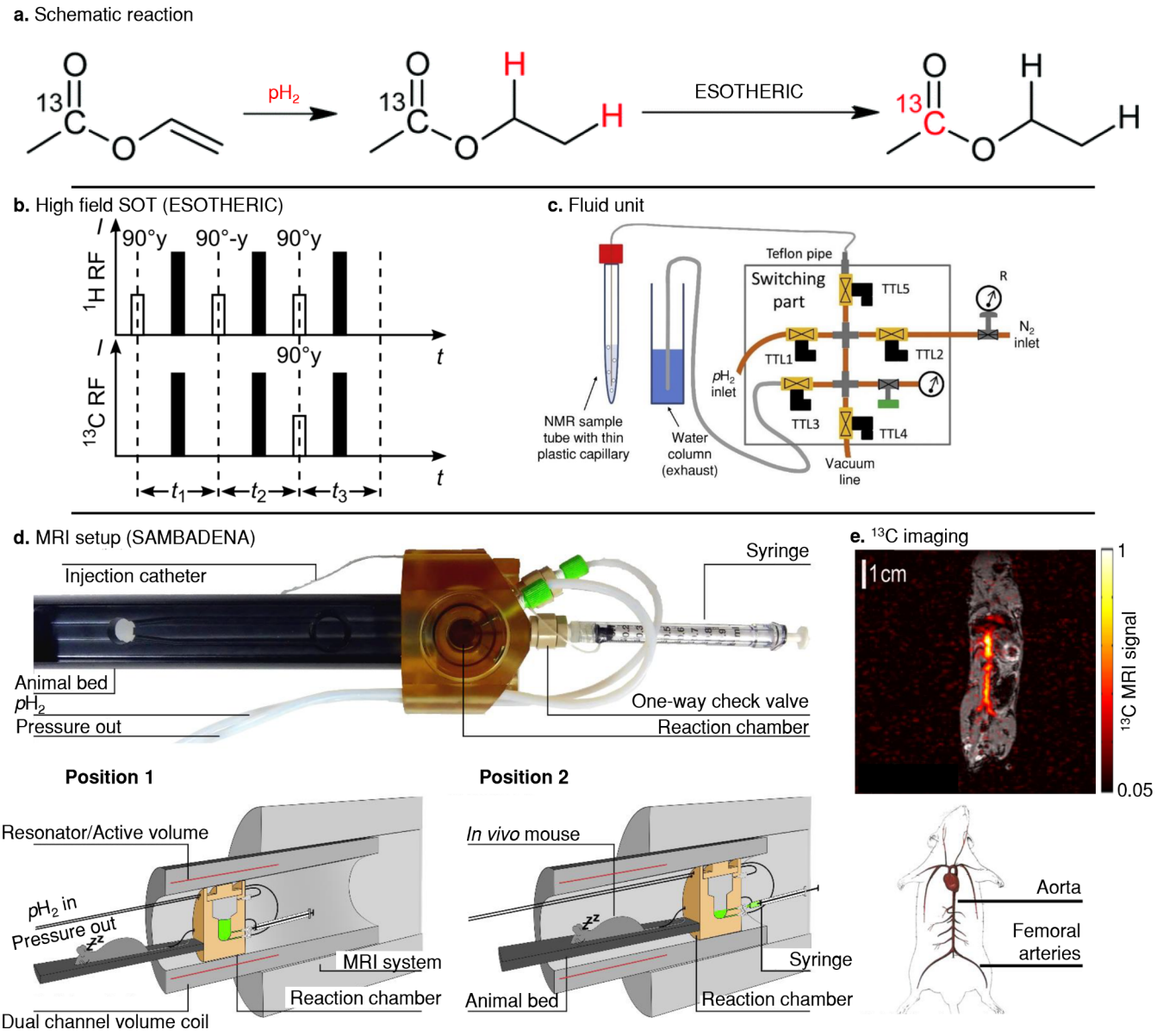

Figure 2. PHIP setups for SOT at constant magnetic fields >1 T, where spin systems are typically in the weak-coupling regime. Schematic view of the hyperpolarization process at high field, where ethyl acetate is polarized by adding pH_2 (a) and spin order transfer with ESOTHERIC (b) or spin-lock induced crossing (SLIC).[214,215] The fluidics are usually handled by a unit consisting of switchable magnetic valves and flow regulation for guiding gases or to apply vacuum to a tube or reactor (c). For MRI systems, dedicated reaction chambers were combined with animal beds allowing animal monitoring, anesthesia, life support, and fast administration of the HP contrast agent (d). As an example, subsecond *in vivo* ^{13}C angiography of a mouse was demonstrated only seconds after the polarization (e), while compatible temperature, pressure, and sterility were assured. Part (a) is reproduced from Pulsed Magnetic Resonance to Signal-Enhance Metabolites within Seconds by Utilizing Para-Hydrogen, Korchak, S.; Yang, S.; Mamone, S.; Glöggler, S., *ChemistryOpen*, Vol. 7, Issue 5, 344−348 (ref 62). Copyright 2018 Wiley. Part (c) is reprinted from *J. Magn. Reson.*, Vol. *285* (Supplement C), Kiryutin, A. S.; Sauer, G.; Hadjiali, S.; Yurkovskaya, A. V.; Breitzke, H.; Buntkowsky, G. A Highly Versatile Automatized Setup for Quantitative Measurements of PHIP Enhancements, pp. 26−36 (ref 95). Copyright 2017, with permission from Elsevier. Parts (d) and (e) are reproduced from In Vivo 13C-MRI Using SAMBADENA, Schmidt, A. B.; Berner, S.; Braig, M.; Zimmermann, M.; Hennig, J.; Elverfeldt, D. von; Hövener, J.-B. *PLoS One*, Vol. *13*, Issue 7, e0200141 (ref 91). Copyright 2018 Public Library of Science.

(*e.g.*, Paravision, LabVIEW,[85−87,93,97] and MATLAB[38,96]).

REVIEW OF PUBLISHED INSTRUMENTS

This section comprises a brief description of instrumentation to produce pH_2, setups for producing HP solutions, HP gases, purification methods, and translation. The section on setups to produce HP liquids is structured by the magnetic field B_{SOT}, where the SOT takes place.

Parahydrogen Generators. As a manifestation of the generalized Pauli exclusion principle, hydrogen molecules exist as two different nuclear spin isomers: the triplet spin states, called oH_2, and the singlet spin state, called pH_2. The energy separation between the ground states of pH_2 and oH_2 is 170.6 K.[83] Hence, in thermal equilibrium at low temperatures (below 25 K), almost all hydrogen molecules are in the singlet state, *i.e.*, nearly pure pH_2. Note that the temperature determines the achievable pH_2-fraction f_{pH2}.

https://doi.org/10.1021/acs.analchem.1c04863
Anal. Chem. 2022, 94, 479−502

The production of pH_2 is straightforward: letting hydrogen gas flow over an ortho-para conversion catalyst at low temperatures results in enriched pH_2. Common conversion catalysts are granular materials with high surface area, such as FeO(OH),[28,29,98] nickel sulfate,[99] or chromic oxide (CrO_3) supported on silica gel.[100] Activated charcoal has been used as an ortho-para conversion catalyst in early works, but the efficiency appears to be lower than for the ferromagnetic oxide materials, especially at high flow rates. The catalytic effect originates from (ferro- or para-) magnetic properties, which induce highly inhomogeneous local magnetic fields that accelerate ortho-para conversion.[36]

The published pH_2 generator designs offer different properties with respect to cost, pH_2-fraction, pressure, flow rate, and ease of use. Aside from commercial products (Bruker BPHG 90, XeUS Technologies LTD, HyperSpin Scientific UG, Advanced Research Systems, IDB Budzylek), many designs for home-built generators have arisen over the last decades. In particular, three primary coolant technologies dominate: single-stage or dual-stage closed-cycle helium cryostats operating at 13.5 to 40 K,[29,36,101−105] liquid helium dewars at 14 to 30 K,[99,100,106,107] and liquid nitrogen dewars at 77 K.[17,98,108−112] Consequently, a dual stage or liquid-helium-based pH_2 generator can practically reach enrichments approaching 100% and a liquid-nitrogen-based pH_2 generator enrichments of up to 52%, respectively. In a liquid N_2 generator pumped below ambient pressure, the enrichment can be increased by lowering the temperature further, *e.g.*, to 63 K at 21 mbar allowing a pH_2 fraction of ≈65%.[113]

The quantification of the pH_2 enrichment can be done optically (*e.g.*, Raman) or by NMR spectroscopy. Raman spectroscopy is about 500 times faster than NMR and does not require a reference sample since it detects both oH_2 and pH_2 directly.[111] However, NMR spectroscopy is generally the quantification method of choice since it is already available in the MR laboratories where PHIP experiments are carried out. The details of quantification have been reviewed thoroughly previously.[114]

Spin Order Transfer (SOT). *SOT Conditions.* In PASADENA experiments, the hydrogenation reaction, observation, and SOT take place at the high magnetic field of an NMR or MRI system (≈ Tesla). If pH_2 is added at chemically nonequivalent sites, I_1 and I_2 typically become weakly coupled (Figure 2a). The strongly coupled case is typically only present if $\delta\nu \approx 0$.[39,115]

For the former case, PHIP ^{1}H signal can be observed as antiphase peaks by a simple 45° excitation. Alternatively, spin order can be converted into in-phase magnetization using RF pulse sequences[116−118] which also enables detection in inhomogeneous B_0 fields.[119,120] However, the first in-phase PHIP ^{1}H spectra were obtained by Pravica et al. by field cycling (ALTADENA),[49] an approach that has also enabled polarization transfer to ^{19}F.[50]

Several techniques have been published to convert $I_{1z}I_{2z}$ into observable magnetization of X-nuclei (often ^{13}C). Here, most RF-SOT sequences are adaptations of the insensitive nuclei enhanced by polarization transfer (INEPT) sequence that considers initial $I_{1z}I_{2z}$ spin order, Figure 2b.[59,121] After the early work from Haake, Natterer, and Bargon, who introduced the pH_2 INEPT+ (phINEPT+) sequence,[60] l-PHINEPT+,[51] selective excitation of polarization using PASADENA (SEPP) INEPT,[122] selective-90 (s90) phINEPT,[54,123,124] and efficient SOT to heteronuclei via relayed INEPT chains (ESOTERIC, Figure 2b)[62,82] sequences were suggested. Note that depending on the spin system, and neglecting relaxation, all RF-SOT schemes can yield ∼100% ^{13}C-polarization, in principle, except phINEPT+, which has a theoretical maximum of ∼50% because of the initial 45° ^{1}H pulse.[38,125] If the initial spin order is $\mathbf{I_1 \bullet I_2}$, different SOT schemes are required, *e.g.*, Goldman's sequence[42] for succinate obtained by reacting a fumarate precursor molecule.[39,48] Additional RF-SOT techniques for strongly coupled protons will be introduced in the next section (SOT at millitesla fields). Adiabatic passages through level anti crossings (also referred to as avoided crossings) were shown to be efficient for the transfer of singlet pH_2 spin order to ^{13}C polarization.[126−128]

Published Setups. Various setups for performing PHIP in NMR[95,123] and MRI systems have been described.[38,91] Such implementations offer the advantage that parts of the sophisticated MR machines, including NMR excitation and acquisition and highly homogeneous field over a large volume, can be employed in the hyperpolarization process. Typically, the NMR or MRI system offers TTL outputs that allow control of the fluid path directly from within the pulse program.

To perform the hyperpolarization in an NMR system, Kiryutin et al. introduced a setup consisting of several valves for supplying gases or liquids, *e.g.*, a cleaving agent to convert a precursor into the desired metabolite.[95] Using standard 5 mm or 10 mm NMR tubes for hydrogenation, SOT, detection, and purification, the system can be implemented in all standard and benchtop NMR spectrometers and has been done so by many laboratories (Figure 2c).[62,120,123,129,130] For *in vivo* imaging, the HP contrast agent has to be transferred to an imaging system.

Performing hyperpolarization within the bore of an MRI system allows *in vivo* imaging only seconds after the hydrogenation (SAMBADENA). Here, the hydrogenation takes place in a reactor enclosed in a dual tune, transmit-receive ^{1}H/^{13}C volume coil, equipped with a local receive coil, for RF-SOT and *in vivo* MRI.[38] The reactor was mounted on the animal bed (with animal warming, vital sign monitoring, anesthesia) such that the contrast agent was delivered directly into a syringe for injection at high field, Figure 2e.[91] *In vivo* imaging of a sterile solution of hydroxyethyl [1-^{13}C]-propionate-d_3 within 15 s after hyperpolarization was demonstrated (Figure 2f), although no purification (*i.e.*, catalyst filtering) was performed.[91]

Published Agents. High ^{13}C polarizations for highly concentrated molecules have been demonstrated with phINEPT+ and ESOTERIC sequences and SAMBADENA.[38,120,129] Promising PHIP agents that were produced at high field with polarization above 10% are tetrafluoropropyl [1-^{13}C]propionate-d_3 (TFPP),[131] [1-^{13}C]succinate-d_2,[39,48] and [2-^{13}C]pyruvate.[132] The latter was achieved using PHIP-SAH, ESOTERIC, and subsequent cleavage of the side arm of cinnamyl [2-^{13}C]pyruvate. Remarkable polarizations were also achieved for other promising PHIP-SAH molecules, namely, ethyl [1-^{13}C]acetate[120,129] and cinnamyl [1-^{13}C]pyruvate.[62,82]

Challenges. The main challenges of *in situ* polarizer setups such as SAMBADENA are due to the limited space within the bore of the MRI or NMR magnet: accommodating production, purification, QA, and the administration within a small volume is not an easy task. RF-SOT sequences, theoretically, achieve ≈100% ^{13}C-polarization but only in fully ^{2}H-labeled molecules, as additional *J*-couplings will interfere (neglecting relaxation).[38,54,123,129,130] In NMR spectrometers, radiation damping can disturb the SOT, while the limited RF power is a serious

https://doi.org/10.1021/acs.analchem.1c04863
Anal. Chem. 2022, 94, 479−502

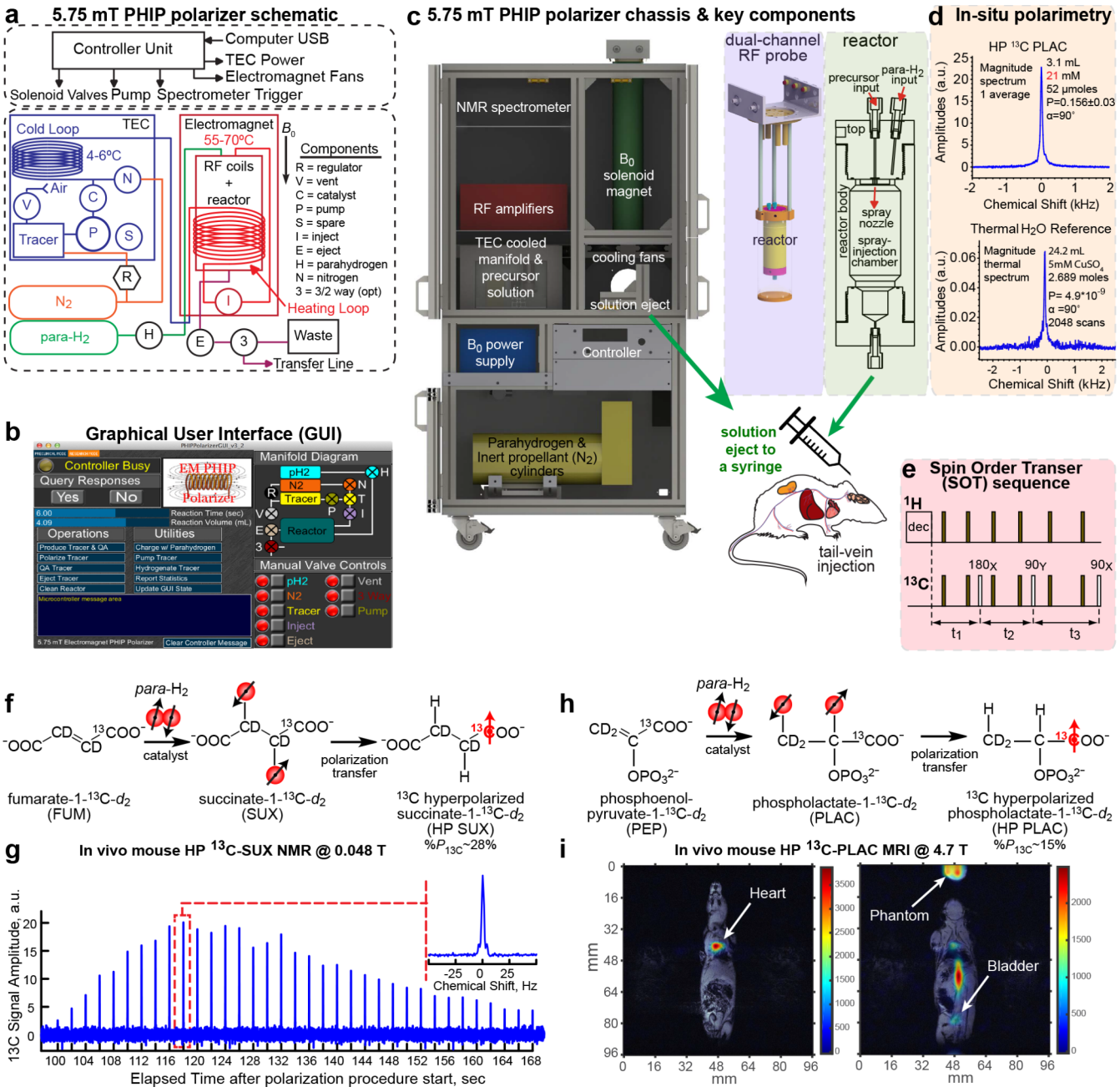

Figure 3. Setups and examples for PHIP at millitesla fields: Overall schematic (a), graphical user interface (b), and rendering (c) of a 5.75 mT automated, preclinical, open-source PHIP polarizer. A dual-channel, $^{1}H/^{13}C$ RF coil was placed inside a B_0 solenoid electromagnet (c, left), and a spray-injection reactor was nested inside the coil. *In situ* NMR detection at ~62 kHz enabled RF calibration and quantification of ^{13}C polarization with respect to thermally polarized water (d). During the hydrogenation reaction of a few seconds, ^{1}H-decoupling was applied to preserve **I·S** spin order and before the polarization was transferred to ^{13}C using the sequence proposed by Goldman et al. (e) Note that there are only three "effective" pulses (white) used while the others (gray) are for refocusing of the Zeeman evolution only. Reaction scheme (f) and *in vivo* ^{13}C NMR (g) of contrast agent SUX detected at low magnetic fields (~0.048 T). Reaction scheme (h) and *in vivo* ^{13}C MRI imaging (i) of contrast agent PLAC at 4.7 T: ^{13}C-MRI (color) was acquired approximately 5−10 s after the injection of ~0.2 mL, ~30 mM hyperpolarized PLAC into the tail vein of a healthy nude mouse (prior to tumor implantation) and overlaid on representative ^{1}H images (gray scale, ^{13}C: GRE, 3 × 3 mm^2 in-plane resolution, 6 mm slice thickness, FOV = 96 × 96 mm^2). Parts (a−d), (h), and (i) are reproduced from Coffey, A. M.; Shchepin, R. V.; Truong, M. L.; Wilkens, K.; Pham, W.; Chekmenev, E. Y. Open-Source Automated Parahydrogen Hyperpolarizer for Molecular Imaging Using 13C Metabolic Contrast Agents. *Anal. Chem.* **2016**, *88*, 8279−8288 (ref 86). Copyright 2016 American Chemical Society. Further permissions related to the material excerpted should be directed to the ACS. Parts (f) and (g) reprinted from *J. Magn. Reson.*, Vol. *281* (Supplement C), Coffey, A. M.; Feldman, M. A.; Shchepin, R. V.; Barskiy, D. A.; Truong, M. L.; Pham, W.; Chekmenev, E. Y. High-Resolution Hyperpolarized in Vivo Metabolic ^{13}C Spectroscopy at Low Magnetic Field (48.7 mT) Following Murine Tail-Vein Injection, pp. 246−252 (ref 149). Copyright 2017, with permission from Elsevier.

concern in MRI setups[120,133−135] because of the large excitation bandwidth needed.[136] Moreover, translational

https://doi.org/10.1021/acs.analchem.1c04863
Anal. Chem. 2022, 94, 479−502

motion of the molecules in the inhomogeneous field of the relatively large reaction chamber in an MRI during SOT can reduce the polarization.[137]

SOT at Millitesla Fields. *SOT Conditions.* The characteristic feature of SOT in the millitesla range is the strongly coupled regime ($\delta\nu \ll J_{1|12}$). Typically, the pairwise pH_2 addition takes place under proton decoupling at B_{SOT}, in part to reduce relaxation, but also to preserve the $\mathbf{I_1 \bullet I_2}$ spin order (Figure 3f,h). After the decoupling, RF-SOT sequences are used to transfer the spin order to a ^{13}C nucleus. A wide range of efficient pulse sequences have been reported[51,57,58] to accomplish polarization transfer in millitesla field range including the pioneering sequence developed by Goldman and co-workers (Figure 3e).[42,83]

Published Setups. As the ^{13}C hyperpolarization can persist for several minutes, the contrast agent can be transferred from the polarizer to the detector without overwhelming loss, *e.g.*, for polarimetry (*i.e.*, measuring the degree of induced polarization) or ultimate application (*i.e.*, *in vivo* imaging). As a result, several millitesla setups with the main static magnetic field ranging from 1.7 mT[89,90] to 50 mT were developed and reported.[85]

The use of the low magnetic field offers certain advantages: (1) the field can be generated by inexpensive electromagnets, resulting in an overall cost-efficient, portable setup;[93] (2) susceptibility effects are low, and B_0 inhomogeneities can be compensated for by magnet design,[93] shims, and sufficiently strong RF pulses. Utilizing an electromagnet has allowed SOT over large reaction volumes, up to 100 mL were reported,[90] enabling the production of clinical-scale doses of ^{13}C-hyperpolarized contrast agents.[83]

These translational advantages were likely decisive for Amersham Biosciences, a healthcare company, to choose this approach for the first commercial prototype. *In vivo* feasibility studies using the Amersham polarizer have been reported extensively.[42,69,83,138] The overall design of the Amersham polarizer was not reported in detail,[42,83,84,139] but several closely related PHIP millitesla polarizer designs were subsequently reported.[36,85−87,89,90,92−94,97]

As described above, the lifetime of the pH_2-derived ^1H spin order is on the order of seconds, and hence, for effective ^{13}C HP, the hydrogenation needs to be completed quickly.[36,140] In practice, fast hydrogenation is achieved through the use of a reactor pressurized to ∼10 bar with pH_2 followed by a spray injection of a hot stream of precursor solution into the chamber.[89,90] For biomedical applications, the reaction is performed in aqueous media employing water-soluble PHIP catalyst at elevated temperature (70−95 °C).[36,86,89,90,139] As a result, the entire bolus of the precursor molecule can be reacted quickly (in a few seconds), i.e., on a time scale that is faster or similar to the decay of the $\mathbf{I_1 \bullet I_2}$ spin order.

The experimental hardware for the hyperpolarization process is relatively similar among reported millitesla PHIP polarizers (Figure 1). By definition, such a system employs a B_0 magnet operating in the millitesla range with typical field strength of 2−9 mT,[36,86,89,90] although the use of higher field (48 mT) permanent magnets have been reported.[85] A large-volume (∼300 mL) dual-channel RF probe is placed inside the magnet to deliver ^1H and ^{13}C RF pulses for the SOT sequence. The high-pressure reactor is nested inside the dual-channel RF coil; Figure 3c shows an example of such an electromagnet-based polarizer. A millitesla-PHIP polarizer is typically connected to (or contains) cylinders of compressed ultra-high-purity (>99.999% or 5.0) pH_2 and inert propellant gas (N_2 or Ar). A series of high-pressure valves and tubes form a manifold (Figure 3a) to fill the reaction chamber with pH_2.[141] This step is followed by the injection of hot precursor solution into the chamber through a nozzle using an inert propellant gas. Various setups were designed to inject a prescribed amount of the precursor solution into the reaction chamber and to eject the HP contrast agent into a receiver ready for transfer and *in vivo* MRI. Although specialized heaters can be employed to control the reaction temperature, the design shown in Figure 3c employs heating generated by a >100 W electromagnet.

Several approaches were developed to orchestrate the interplay of actuating multiple valves and playing out the RF-SOT, usually including software and a hardware interface (LabVIEW-,[36,90,96,97] Arduino-,[86] MATLAB,[96] and NMR spectrometer based[87]). A typical graphical user interface (GUI) allows setting various parameters (reaction time, precursor dose), choosing the SOT sequence, actuating individual valves, and executing various polarization or maintenance routines and sometimes performing NMR (Figure 3b, open-source Arduino-based controller software).[86] All published controller designs have their own merits.

To achieve high and reliable polarization through robust device operation, the accurate and precise application of the RF-SOT is critical.[51] Optimal RF-SOT performance requires calibrated B_1 power and transmission resonance frequencies for both RF channels in particular. Performing these calibrations *in situ* by detecting NMR signal in the reaction chamber using a transmit-receive polarizer design drastically facilitates these procedures. *In situ* calibrations, however, are not necessarily needed to produce the HP agents, because an external (*i.e.*, *ex situ*) NMR spectrometer, MRI scanner, or a low-field polarimetry station may be employed for the calibrations[89] and for probing the achieved ^{13}C polarization level.[69] This so-called transmit-only design is less complex and typically result in a lower device cost as no extra NMR receiver hardware is needed. The transmit RF pulses can be generated using simple waveform generators (*e.g.*, NI, Austin, TX), consumer-grade RF amplifiers (WRAT, Onkyo, Osaka, Japan), and untuned RF coils with a low Q factor, mitigating radiation damping issues noted in the above section.

The hyperpolarizers employing transmit-receive design were realized by using a commercial, low-frequency, dual-channel NMR spectrometer and dual tune transmit-receive coil (*e.g.*, Kea2, Magritek).[86,87] In another approach, a geometrically decoupled, single or dual tuned receive coil was added to the untuned transmit coil, using the same low-cost waveform generators, amplifiers, and ADC/DAC hardware as for the transmit-only design described above.[93,96]

These transmit-receive designs allow using the signal of thermally polarized water to calibrate B_0 and B_1.[86,87,93,96,142] As the polarization of HP samples is independent of the detection field, a high signal-to-noise ratio (SNR) spectrum was readily obtained in *in situ* low-field polarimetry as shown for the HP contrast agent [1-^{13}C]phospholactate-d_2 (PLAC) at ∼62 kHz (Figure 3d).

While transmit-receive designs are more complex and can be more expensive (by ∼$30 000 for the Kea2), calibration is relatively straightforward, and good reliability and reproducibility of the hyperpolarization yield is achieved. The efficiency of SOT can be improved further by reducing the complexity of the spin system. For example, deuteration was used to simplify

https://doi.org/10.1021/acs.analchem.1c04863
Anal. Chem. 2022, 94, 479−502

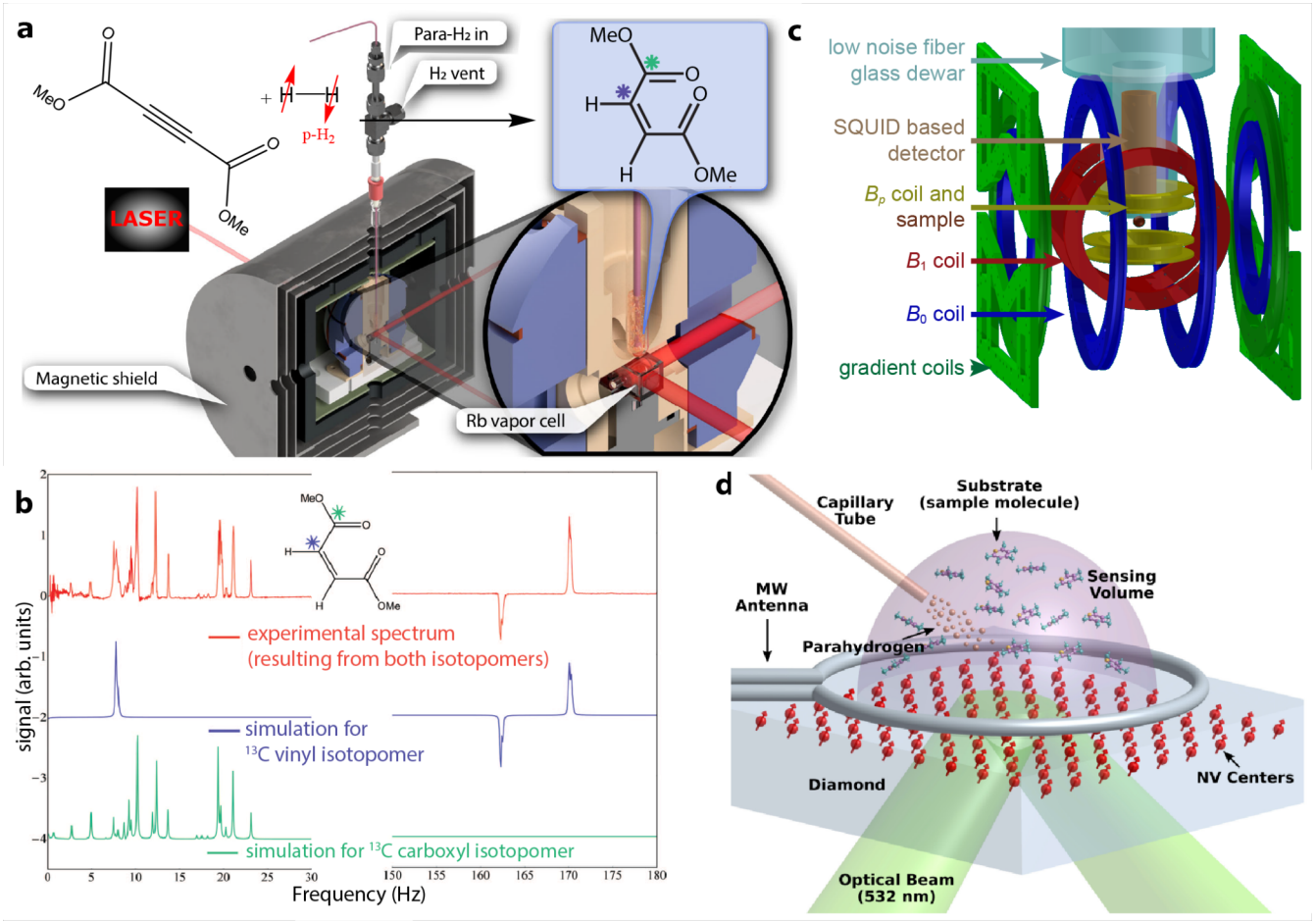

Figure 4. Setups and examples suitable for PHIP at ULF: (a) atomic magnetometer system based on a Rb vapor cell, (b) PHIP enhanced zero field NMR spectrum of dimethyl maleate acquired with a Rb vapor magnetometer, (c) SQUID based system, and (d) optically probed nitrogen-vacancy (NV)-NMR spectrometer. Part (a) is reproduced from Toward Large-Scale Steady-State Enhanced Nuclear Magnetization with in Situ Detection, Blanchard, J. W.; Ripka, B.; Suslick, B. A.; Gelevski, D.; Wu, T.; Münnemann, K.; Barskiy, D. A.; Budker, D. *Magn. Reson. Chem.*, **2021**, *59*, 1208 (ref 171). Copyright 2021 Wiley. Part (b) is reprinted from Parahydrogen-Induced Polarization at Zero Magnetic Field, Butler, M. C.; Kervern, G.; Theis, T.; Ledbetter, M. P.; Ganssle, P. J.; Blanchard, J. W.; Budker, D.; Pines, A., *J. Chem. Phys.*, **2013**, Vol. *138*, Issue 23, 234201 (ref 154), with permission of AIP Publishing. Part (c) is reprinted from Mutual Benefit Achieved by Combining Ultralow-Field Magnetic Resonance and Hyperpolarizing Techniques, Buckenmaier, K.; Rudolph, M.; Fehling, P.; Steffen, T.; Back, C.; Bernard, R.; Pohmann, R.; Bernarding, J.; Kleiner, R.; Koelle, D.; Plaumann, M.; Scheffler, K., *Rev. Sci. Instrum.*, **2018**, Vol. *89*, Issue 12, 125103 (ref 170), with permission of AIP Publishing. Part (d) is reproduced from Micron-Scale NV-NMR Spectroscopy with Signal Amplification by Reversible Exchange, Arunkumar, N.; Bucher, D. B.; Turner, M. J.; TomHon, P.; Glenn, D.; Lehmkuhl, S.; Lukin, M. D.; Park, H.; Rosen, M. S.; Theis, T.; Walsworth, R. L., *PRX Quantum*, Vol. 2, Issue 1, 010305 (ref 172). Copyright 2021 American Physical Society.

HEP, SUC, and PLAC to an effective 3-spin-1/2 system (two nascent protons and one ^{13}C nucleus), which increased the final ^{13}C polarization for PLAC to 15% versus 1% for the fully protonated variant, Figure 3h.[53,143] While deuterium (and phosphorus-31) nuclei possess a spin, they are not excited by the RF and hence not effectively involved in the SOT.[42] In favorable cases, P_{13C} of more than 20% was achieved with millitesla polarizers,[36,42,139] *e.g.*, P_{13C} = 28% for [1-^{13}C]-succinate-d_2 (SUX, Figure 3f). Despite the enormous signal enhancement provided by hyperpolarization, metabolic imaging with HP contrast agents usually results in limited-SNR images. Thus, it is not surprising that only deuterated precursors with high P_{13C} were translated to *in vivo* studies using millitesla PHIP polarizers so far.[69,83,86,89,90,144−150]

To date, millitesla-polarizers were employed for *in vivo* ^{13}C MRI or MRS with SUX,[149,151] SUX esters,[147] HEP,[5,69,152] TFPP,[145] and PLAC,[86] Figure 3g,i. Thorough reviews covering the *in vivo* applications can be found elsewhere.[114,153]

Two interesting developments, which broaden the scope of polarizable molecules drastically, are PHIP-SAH[19] and PHIP-X.[26] The experimental realizations of these techniques will be described in more detail below, but the millitesla polarizers described here appear to be well positioned for these emerging protocols.

Challenges. The millitesla PHIP polarizers have been shown to be successful devices for the efficient production of HP ^{13}C contrast agents in aqueous media with high P_{13C} exceeding 25% for *in vivo* applications. Using PHIP-SAH molecules may dramatically enlarge the pool of agents, *e.g.*, to ^{13}C-labeled pyruvate. Despite this success, however, all *in vivo* translated precursors so far require deuterated substrates in addition to ^{13}C labeling. While deuteration offers the benefit of a prolonged polarization lifetime, it also increases the cost and the complexity of synthesis of the precursors, which is a clear drawback compared to MFC-SOT. No millitesla polarizer incorporating a purification unit has been presented so far.

https://doi.org/10.1021/acs.analchem.1c04863
Anal. Chem. 2022, 94, 479−502

SOT at Ultralow Fields (ULF). *SOT Conditions.* At ultralow fields (micro- or nanotesla), the frequency differences between heteronuclei and protons (γ_{1H}-γ_X) are reduced to be on the order of the *J*-couplings or below. At such low fields, a spin bath between all spin−spin coupled nuclei is effectively established through which polarization can easily propagate spontaneously. In other words, if a part of a nuclear spin network is initialized in the singlet state via pH_2 and the Zeeman interactions are negligible compared to the *J*-couplings, then the polarization spreads through the network.[154,155] The beauty of this "spontaneous" polarization transfer approach is that it is general and does not require specialized pulse sequences that are highly dependent on the specific spin system under study. Note that this concept was realized early on, when the so-called ALTADENA approach was established,[49] where pH_2 was introduced into the spin system through hydrogenation and polarization "flows" to other ^{1}H spins at millitesla fields or below,[156] as mentioned in the section above and is as theoretically analyzed in the following section. However, to polarize a spin-1/2 heteronucleus, such as ^{13}C, ^{15}N, ^{31}P, *etc.*, ultralow microtesla fields are required to strongly couple the protons of the spin system with the target X-nucleus to allow spontaneous polarization transfer. Over the past decade, a wide variety of experiments have been demonstrated taking advantage of this heteronuclear spin bath at microtesla fields, including hydrogenative[19,126,157−162] and non-hydrogenative PHIP.[163−166] The newest approaches have used pulse sequences at microtesla fields,[127,167−169] which can focus polarization transfer in a more targeted way to specific nuclei but become highly dependent on the specific spin system under study.

Published Setups. While dedicated setups to produce diagnostically relevant contrast agent have not yet emerged, some interesting setups were described that allow exploiting the unique properties at these fields. Among these are (a) the distribution of the polarization across an entire molecule and different coherences,[107] (b) the unique sensors to detect signals in the Hz−kHz range,[170−172] and (c) the identification of molecules by their *J*-couplings rather than their chemical shift.[173−175]

To establish magnetic fields below the Earth's field, entering nanotesla to microtesla field regimes, typically mu-metal shields are used.[170,176] Inside such shielding, well-defined magnetic fields are commonly generated with conventional resistive coils in Helmholtz, solenoid, or other configurations driven by low noise current sources.

To acquire HP spectra (typically from small molecules in solution), a variety of ULF MR setups have been designed, Figure 4. The detection sensitivity for conventional RF coils, as used for high field MR experiments, decreases with frequency.[177] Therefore, at ultralow fields, different magnetic field detectors such as atomic magnetometers (Figure 4a)[154,155,171,176,178,179] or superconducting quantum interference devices (SQUIDs) (Figure 4b)[170,180] may be more sensitive than inductive detection. Such sensors are even sensitive enough to perform magnetoencephalography[181] but can also be used to detect nuclear spins. They can operate as broadband detectors (SQUIDs: DC, ≈1 GHz; atomic magnetometers: DC, ≈1 kHz), where no matching and tuning is required and the MR signal of different nuclei such as ^{13}C, ^{15}N, ^{19}F, and ^{1}H can be detected simultaneously.[107]

More recently, fluorescent nitrogen vacancy (NV) centers in diamonds (Figure 4c) have also been used to detect PHIP signal. While the NV centers typically have less absolute magnetic field sensitivity, the advantage is that they can be brought in direct contact with the solution (unlike SQUIDS or atomic magnetometers).[172,182] These can also be used for magnetometry at zero field.[183]

The linewidth of the detected MR signals for ULF setups can be less than 1 Hz down to tens of mHz,[173] so that *J*-couplings can be easily resolved. Narrow line widths are obtained since field inhomogeneities decrease with the field strength, which enables chemically specific, high resolution *J*-coupling spectroscopy.

Challenges. Generating and detecting HP signals at ULF offers unique insights into the investigated spin systems and provides NMR and MRI without requiring superconducting magnets. However, a disadvantage of all ULF detection methods remains, which is the frequency-dependent noise of the sensors (SQUIDs ≈ 1 $fT/Hz^{1/2}$, atomic magnetometers ≈10 $fT/Hz^{-1/2}$). Accordingly, there is an ongoing quest to decrease the noise level below the sample noise. Moreover, medically viable polarizers or sensors that take advantage of PHIP at ULF have not emerged yet. The aspiration remains that the described discoveries and techniques will soon be translated into broad applications.

Magnetic Field Cycling (MFC). *SOT Conditions.* MFC is another method that is widely used for the polarization transfer from the $\mathbf{I_1 \bullet I_2}$ spin order to heteronuclei. In contrast to the previous sections, which dealt with SOT at a constant magnetic field B_0, MFC exploits varying the magnetic field from values close to the geomagnetic field (30−50 μT) to nearly zero field and a few tesla. MFC-SOT was the first method to produce net ^{1}H magnetization[49] and used to produce the first ^{13}C HP contrast agents for *in vivo* MRI in 2001.[5] The method is not to be confused with the fast field cycling relaxometry where the magnetic field is varied to investigate relaxation or spin-state evolution at a low magnetic field in order to gain information about physical or chemical properties of the system under study.[184] For PHIP, a MFC process does not explicitly require *in situ* signal detection, although some setups do this.[88]

To give an idea of the effect of MFC on the spin state populations in PHIP-polarized molecules, we consider a three-spin system formed by two pH_2 protons (H and H′) and a heteronucleus (X). The spin states can be conveniently described using the singlet-triplet-Zeeman basis. The eight basis states are

$$|T_+\alpha\rangle = |\alpha\alpha\alpha\rangle,\ |T_+\beta\rangle = |\alpha\alpha\beta\rangle,$$

$$|T_0\alpha\rangle = \frac{1}{\sqrt{2}}|(\alpha\beta + \beta\alpha)\alpha\rangle,\ |T_0\beta\rangle = \frac{1}{\sqrt{2}}|(\alpha\beta + \beta\alpha)\beta\rangle,$$

$$|S_0\alpha\rangle = \frac{1}{\sqrt{2}}|(\alpha\beta - \beta\alpha)\alpha\rangle,\ |S_0\beta\rangle = \frac{1}{\sqrt{2}}|(\alpha\beta - \beta\alpha)\beta\rangle,$$

$$|T_-\alpha\rangle = |\beta\beta\alpha\rangle,\ |T_-\beta\rangle = |\beta\beta\beta\rangle$$

where the first letter refers to the proton spin state, and the second refers to the heteronuclear spin state.

Upon pH_2 addition to a precursor at geomagnetic fields, the states $|S_0\ \alpha\rangle$ and $|S_0\ \beta\rangle$ are populated almost equally. At these "higher" fields, the ^{1}H and heteronuclei are weakly coupled and no heteronuclear magnetization is obtained, because to a good approximation only the $|T_0\ \alpha\rangle$−$|S_0\ \alpha\rangle$ states and the $|T_0\ \beta\rangle$−$|S_0\ \beta\rangle$ states are mixed. However, when the magnetic field is low enough such that the difference in proton and heteronuclear

https://doi.org/10.1021/acs.analchem.1c04863
Anal. Chem. 2022, 94, 479−502

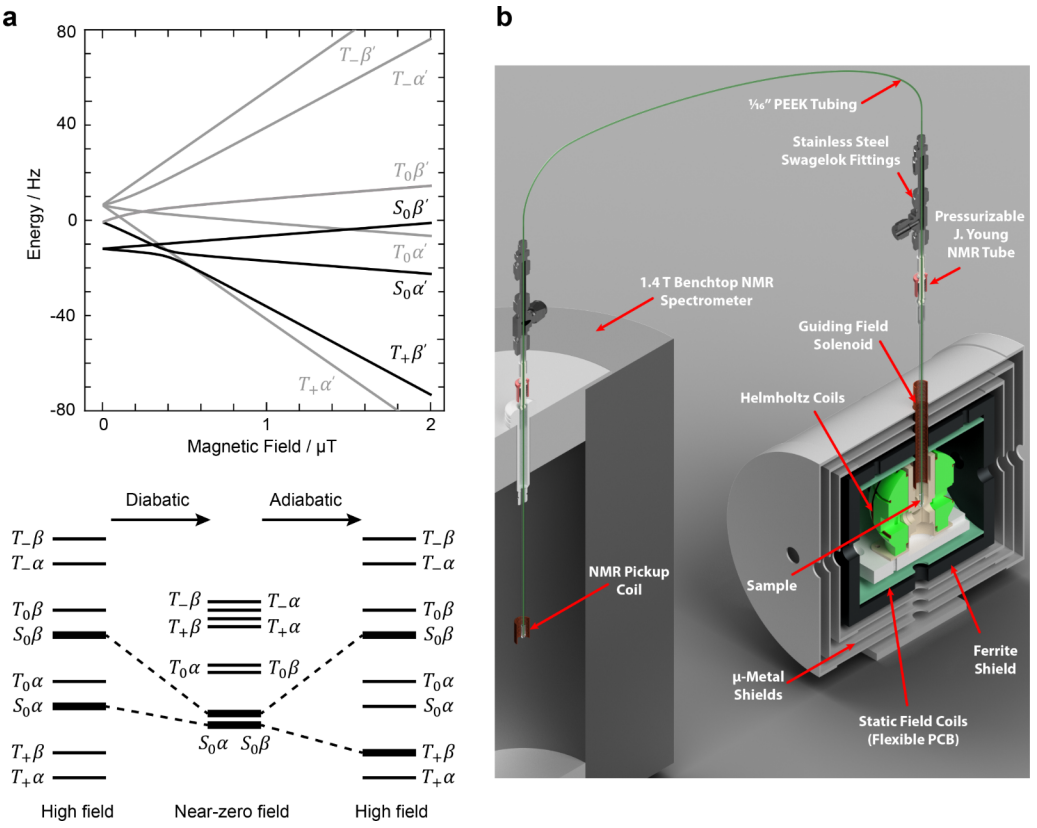

Figure 5. Diagrams and setups for PHIP by magnetic field cycling (MFC). (a) Energies of the eigenstates of [1-^{13}C]fumarate, plotted as a function of magnetic field strength, with states relevant to MFC-SOT highlighted in black (top). In an ideal MFC, the pH_2-derived singlet order $\mathbf{I}_1\cdot\mathbf{I}_2$ is converted into heteronuclear magnetization by the first diabatic passage to the near-zero-field, followed by adiabatic passage back to the microtesla field (bottom). The diabatic passage preserves the state of the system with the protons in a singlet state (*i.e.*, $|S_0\alpha\rangle$ and $|S_0\ \beta\rangle$), but during the subsequent adiabatic return to the high field, the state $|S_0\alpha\rangle$ evolves into $|T_+\beta\rangle$, meaning some degree of proton singlet order is lost, but heteronuclear polarization in the β state is gained. (b) Illustration of a polarizer where a sample is polarized by MFC or field sweeping and transferred to an NMR system for detection. Figure reprinted from Polarization Transfer via Field Sweeping in Parahydrogen-Enhanced Nuclear Magnetic Resonance, Eills, J.; Blanchard, J. W.; Wu, T.; Bengs, C.; Hollenbach, J.; Budker, D.; Levitt, M. H., *J. Chem. Phys.*, **2019**, Vol. *150*, Issue 17, 174202 (ref 158), with permission of AIP Publishing.

Larmor frequencies approximately matches the *J*-coupling frequencies, the states with equal angular momentum projection along the field axis (z): $|T_+\ \beta\rangle$, $|T_0\alpha\rangle$, $|S_0\alpha\rangle$, and $|T_-\alpha\rangle$, $|T_0\beta\rangle$, $|S_0\beta\rangle$ are mixed. This leads to level anticrossings (LACs) between the relevant states, and by varying the magnetic field either rapidly (diabatic passage) or slowly (adiabatic passage), it is possible to transfer spin state populations between the eigenstates.[185] The spin state energies and populations are shown in Figure 5a, and the relevant Hamiltonians are reported in ref 158.

In the most common example of MFC, the hydrogenation reaction using pH_2 is carried out in the laboratory field (usually tens of microtesla), which is high enough to prevent leakage of proton spin order onto heteronuclear spins but low enough that proton chemical shift differences, which would lead to loss of spin order, are suppressed, *i.e.*, the protons remain strongly coupled. The field is then diabatically (rapidly) reduced to near-zero field and then adiabatically (slowly) increased to the laboratory field such that the spin state populations follow the eigenstates as the field passes through the LACs. Overall, this process leads to the $\mathbf{I}_1\bullet\mathbf{I}_2$ order being transformed into both proton and heteronuclear magnetization. For biomedical applications, it is the heteronuclear Zeeman order that is of interest, Figure 5a.

Published Setups. The most basic MFC experiment is a hydrogenation in a few millitesla followed by transfer to a few tesla for detection.[49] To transfer polarization to X-nuclei, a mu-metal chamber can be used to reach near-zero field conditions (nanotesla). The two passages can be achieved manually, by dropping the sample after hydrogenation into the shield (diabatic passage) and lifting it out slowly (adiabatic passage).[5] In more sophisticated setups, the speed of passages is controlled by means of an electromagnet inside the mu-metal shield.[159,186] The use of coils allows more-precise control over the magnetic fields and has become a routine approach for MFC. A schematic of an experimental apparatus used for MFC is shown in Figure 5b.

The approach was first introduced experimentally by K. Golman et al. in 2001.[5,55] After pairwise addition of pH_2, the sample was (rapidly) dropped into a three-layer mu-metal shield at <100 nT and then slowly lifted at approximately 10 cm/s rate. Using this method, the authors generated 4% ^{13}C polarization on [1-^{13}C]maleic acid dimethyl ester. A more thorough theoretical explanation of the technique and description of the setup followed,[55,139] now including coils inside the magnetic shield to provide time-dependent variable fields. The magnetic field was initially held at 100 μT as the hydrogenated sample was inserted into the shield, then diabatically reduced to 30 nT in about 1 ms, and then

https://doi.org/10.1021/acs.analchem.1c04863
Anal. Chem. 2022, 94, 479−502

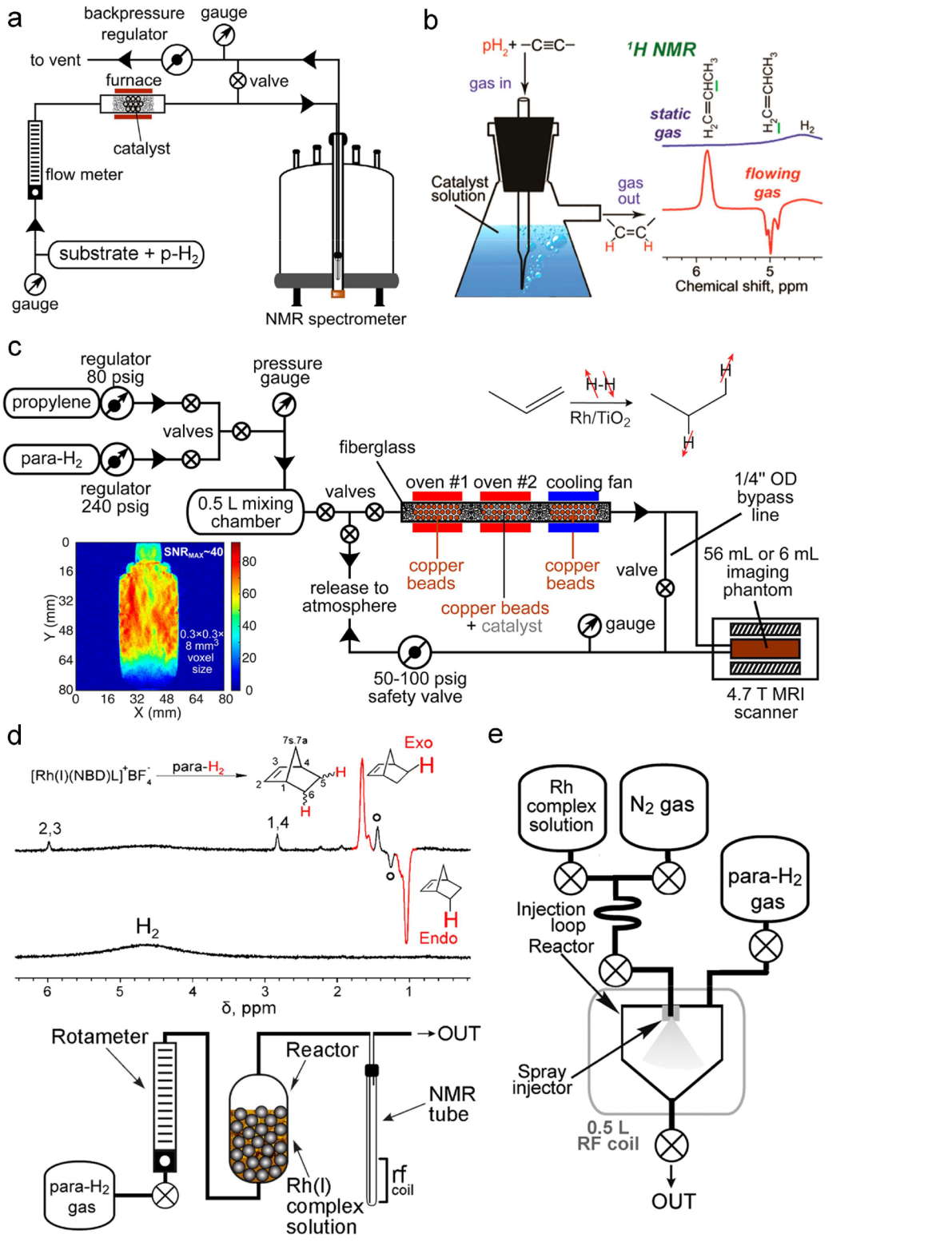

Figure 6. Setups for PHIP of gases. (a) Experimental setup employed for producing hyperpolarized gases or vapors via heterogeneous hydrogenation of unsaturated precursors premixed with pH_2. (b) Schematics of an experimental setup (left) for biphasic hydrogenation of gases upon bubbling their mixture with pH_2 through a homogeneous solution of metal complex catalyst, with the hyperpolarized product continuously escaping into the gas phase. The spectra shown as an example (right) are for biphasic hydrogenation of propyne to propylene. (c) Schematics of a more advanced experimental setup used for a rapid batch-mode production and MRI detection of hyperpolarized propane gas. The insets show the reaction scheme (top-right) and a gradient echo 2D MR image of ~200 mL of hyperpolarized propane gas in a ~56 mL container acquired at 4.7 T (bottom-left). (d) The diagram of the experimental setup used to produce hyperpolarized vapor of norbornene by bubbling pH_2 through an aqueous solution of a Rh(I) complex possessing a norbornadiene ligand (bottom), the reaction scheme (top), and the resulting gas-phase ^{1}H NMR spectra (middle). Open circles label the signals of norbornane. Plastic spheres in the reactor were used to reduce its volume. (e) The diagram of the experimental setup used for injecting Rh(I) complex solution into a 56 mL volume containing pH_2 at ≈7 bar pressure for subsequent *in situ* ^{1}H

https://doi.org/10.1021/acs.analchem.1c04863
Anal. Chem. 2022, 94, 479−502

Figure 6. continued

NMR spectroscopy of hyperpolarized norbornene at 47.5 mT. Part (a) is reproduced from Heterogeneous Parahydrogen-Induced Polarization of Diethyl Ether for Magnetic Resonance Imaging Applications, Salnikov, O. G.; Svyatova, A.; Kovtunova, L. M.; Chukanov, N. V.; Bukhtiyarov, V. I.; Kovtunov, K. V.; Chekmenev, E. Y.; Koptyug, I. V. *Angew. Chem. Int. Ed. Engl.*, Vol. *27*, Issue 4 1316−1320 (ref 198). Copyright 2021 Wiley. Part (b) is reproduced from Kovtunov, K. V.; Zhivonitko, V. V.; Skovpin, I. V.; Barskiy, D. A.; Salnikov, O. G.; Koptyug, I. V. Toward Continuous Production of Catalyst-Free Hyperpolarized Fluids Based on Biphasic and Heterogeneous Hydrogenations with Parahydrogen. *J. Phys. Chem. C* **2013**, *117* (44), 22887−22893 (ref 196). Copyright 2013 American Chemical Society. Part (c) is reproduced from Salnikov, O. G.; Nikolaou, P.; Ariyasingha, N. M.; Kovtunov, K. V.; Koptyug, I. V.; Chekmenev, E. Y. Clinical-Scale Batch-Mode Production of Hyperpolarized Propane Gas for MRI. *Anal. Chem.* **2019**, *91* (7), 4741−4746 (ref 202). Copyright 2019 American Chemical Society. Parts (d) and (e) are reproduced from Kovtunov, K. V.; Barskiy, D. A.; Shchepin, R. V.; Coffey, A. M.; Waddell, K. W.; Koptyug, I. V.; Chekmenev, E. Y. Demonstration of Heterogeneous Parahydrogen Induced Polarization Using Hyperpolarized Agent Migration from Dissolved Rh(I) Complex to Gas Phase. *Anal. Chem.* **2014**, *86* (13), 6192−6196 (ref 195). Copyright 2014 American Chemical Society. Further permissions related to the material excerpted should be directed to the ACS.

exponentially ramped back to 100 μT on the order of seconds. This approach, in combination with a spray-injection chamber for the hydrogenation with pH_2, led to ^{13}C polarization on hydroxyethyl-propionate of ≈21%. In later work, this experimental apparatus was used to produce HP ^{13}C contrast agents for coronary angiography imaging in pigs.[152]

There is merit to the approach of shuttling samples in and out of a magnetic shield by hand in the simplicity and low experimental requirements, and this approach was employed to hyperpolarize various heteronuclei such as ^{13}C,[187] ^{15}N,[188] and ^{129}Si.[189] A few years later, this approach was employed to hyperpolarize the ^{13}C spins in a number of molecules, including pyruvate and acetate, by means of PHIP-SAH.[19,56] A detailed description of a coil-based magnetic field cycling setup was provided by Shchepin et al. where they studied the dependence of ^{13}C polarization in [1-^{13}C]ethyl acetate on the minimum field used during the MFC.[186] They demonstrated that the MFC should reach fields below 1 μT for efficient ^{13}C polarization. Using this optimized coil-based approach, the ^{13}C polarization of [1-^{13}C]pyruvate generated via side arm hydrogenation was improved from 2.3%[19,56] to 8.3%,[159] and the method was also applied for hyperpolarizing [1-^{13}C]-fumarate (FUM).[24,190]

In FUM, derived from hydrogenation of ADC (acetylene dicarboxylate), an AA′X spin system is formed.[191] Because of its simplicity, the system is useful for studying and optimizing MFC methods. It was on this molecular system that an MFC variant known as magnetic field sweeping was tested.[158] In this method, rather than a diabatic field reduction followed by an adiabatic increase, the magnetic field is inverted adiabatically, *i.e.*, passing through a zero field. The field sweeping method was then applied to hyperpolarize vinyl acetate, and the effect of the magnetic field sweep step size and rate was investigated.[88] The authors found that for MFCs using a field range of a few microtesla, a sweep rate of 50 steps/μT/s was sufficient, with higher values leading to no improvement. Magnetic field sweeping does not need rapid field changes and hence seems more amenable for application to liquids under continuous flow. Its lower efficiency with respect to field cycling[158] is likely due to the deleterious effects of transverse magnetic fields when passing through the zero-field point, and hence in future work, an MFC approach was used for generating HP FUM.[24,190]

This molecular system was also used to study the benefits of constant-adiabaticity methods for MFC and field sweeping.[192] Under the constant-adiabaticity constraint, the magnetic field variations are slow at the LAC field, but the field can be varied more rapidly away from this key feature. This is particularly useful for spin systems that relax rapidly during the MFC process.

Challenges. More complicated molecular systems can present some pitfalls to the application of MFC, in particular when quadrupolar nuclei such as ^{2}H[193] or ^{14}N[188] are *J*-coupled to the pH_2-derived protons. The strong-coupling condition that is reached at nearly zero field brings these heteronuclei in contact with the spin order of pH_2 and quadrupolar relaxation can work as a hyperpolarization sink.

Another caveat to be considered is that exposure to magnetic fields magnetizes the mu-metal, and so the magnetic shielding should be periodically degaussed to ensure the near-zero field condition is met inside it. In cases where the magnetic shield is near a high-field magnet, it is common to use active shimming with coils inside the shield to achieve the near-zero field conditions.

PHIP OF GASES

While the low sensitivity of NMR often is an issue, it is particularly severe for gases as their densities at ambient pressure are ∼1000-fold lower compared to liquids. PHIP has been applied to produce HP molecules in the gas phase,[14,15,194] mostly gases but also vapors of volatile liquids and even solids. One approach is to use a solution of a metal complex in a homogeneous hydrogenation with subsequent transfer of the target species to the gas phase. For instance, aqueous stoichiometric hydrogenation of norbornadiene resulted in the release of water-insoluble hyperpolarized norbornene to the gas phase.[195] Bubbling of a mixture of pH_2 with propylene (propyne, *etc.*) through a solution of a rhodium or iridium complex was used to produce polarized gases.[196] Another approach relies on the use of solid catalysts to produce PHIP in heterogeneous hydrogenations (HET-PHIP). By bubbling pH_2 through a suitable volatile liquid, pH_2 is saturated with its vapor, and this gaseous mixture is then supplied to a cell with a solid catalyst for hydrogenation. Often, unsaturated gases premixed with pH_2 are used in HET-PHIP experiments.

Published Setups. Published examples include hydrogenation of vinyl acetate vapors over a Rh/TiO_2 catalyst with subsequent dissolution and hydrolysis of ethyl acetate to hyperpolarized ethanol and acetate,[197] and hydrogenation of vinylethyl ether to hyperpolarized diethyl ether, a known inhalable anesthetic.[198] Unsaturated gases are simply premixed with pH_2 and supplied to a catalytic reactor to yield a continuous stream of hyperpolarized gas.[14,15,194,199]

The experiments with gases can be performed under PASADENA or ALTADENA conditions. For propane ($H_3C-CH_2-CH_3$) produced upon hydrogenation of propy-

https://doi.org/10.1021/acs.analchem.1c04863
Anal. Chem. 2022, 94, 479−502

lene ($H_2C{=}CH{-}CH_3$), in PASADENA experiments, a pair of enhanced antiphase multiplets is observed with an admixture of in-phase contributions of opposite sign for the two signals. In ALTADENA experiments with hydrogenation at the Earth's field, where all ^1H spins in a product molecule are strongly coupled, transfer of the gas to the NMR probe results in the observation of polarization for all coupled ^1H nuclei. For propyne hydrogenation to propylene, it is possible to estimate the stereoselectivity of the hydrogenation by fitting the experimental spectra to ALTADENA numerical simulations, which would be otherwise impossible for this reaction.[200] The adiabatic condition of low-to-high field transfer is seldom met fully with gases as T_1 times are short, and slow transfer leads to major polarization losses. Short relaxation times in the gas phase are due to spin-rotation interaction, which also makes the T_1 of heteronuclei shorter than for protons. As a result, polarization transfer from ^1H to heteronuclei is impractical even though its feasibility has been demonstrated.[201]

PASADENA experiments with gases are particularly easy to implement; the substrate gas and pH_2 (and, if required, a diluent gas, *e.g.*, N_2) can be premixed in a gas cylinder or supplied by combining the outputs of mass flow controllers and the hydrogenation reaction performed in an NMR tube containing a solid catalyst, its suspension in a liquid, or a solution of a suitable transition metal complex. Continuous-flow ALTADENA experiments, performed using a setup such as the one illustrated in Figure 6a, provide a much broader flexibility in experimental conditions. A reactor can be as simple as a temperature-controlled section of stainless steel or copper tubing or a quartz U-tube containing solid catalyst powder, which is held in place by glass wool plugs. It is important to monitor the reactor bed temperature as hydrogenation is exothermic and run-away heating effects are possible. The gas is supplied via gas lines from a gas cylinder to the reactor and then from the reactor to the NMR tube and eventually toward the exhaust; all connections should be gastight to avoid gas leaks, and all components should withstand the required gas pressures. Commercially available flow NMR probes, popularized with the advent of liquid chromatography (LC) NMR, are well suited for acquiring the spectra on aliquots of the flowing hyperpolarized gases. However, gas flow rates through the smaller coil volumes of these probes need to be reduced accordingly to avoid residence-time line-broadening. Such effects can also be averted with an interrupted-flow system where the gas flow is allowed to bypass the probe during NMR acquisition while not perturbing the steady-state of the reactor bed. This is also a useful way to isolate a gas sample in the probe to acquire thermally equilibrated spectra. A provision for heating the reactor and catalyst pretreatment in a stream of H_2 or gas mixtures is useful. A somewhat more sophisticated setup was designed[202] for a controlled clinical-scale (>300 mL in 2 s) batch production of HP propane (Figure 6c). This systems has provisions for efficient preheating of reactants and subsequent dissipation of heat produced in the highly exothermic hydrogenation reaction as well as for operation at elevated pressures (~8 bar).

HP norbornene vapor was produced from an aqueous solution of Rh(I) complex incorporating a norbornadiene ligand by either bubbling pH_2 through it (for high-field NMR, Figure 6d) or by spraying it into a chamber pressurized with pH_2 (for NMR at 47.5 mT, Figure 6e).[195] Gas-liquid biphasic hydrogenations employed a dissolved catalyst, and gaseous reactants were bubbled through the solution, Figure 6b. The reaction product returned to the gas phase and retained a significant level of hyperpolarization, providing a complete separation of the hyperpolarized substance from the catalyst.[196]

Prepolarized propane was used in many studies to image voids in various objects[203−205] including microfluidic devices.[206,207] Imaging of HP reaction products formed in an operating model catalytic reactor facilitates mapping of their spatial distribution within the catalyst bed.[208−211]

Challenges. The main challenge with gases is the short T_1 time; for propane, it is below 1 s at 9.4 T and 1 bar but depends strongly on pressure and the gas mixture composition.[212] T_1 times tend to be longer for shorter molecular rotational correlation times, *i.e.*, for larger and/or heavier molecules, higher gas pressures, or gases in small pores. The T_1 values of small gas molecules generally increase upon dissolution in liquids. For example, $T_1 \approx 1$ ms for H_2 gas at 1 bar but it increases by ~1000-fold upon dissolution in methanol-d_4. Condensation of hyperpolarized diethyl ether vapor was also shown to prolong its hyperpolarization lifetime.[198] Furthermore, because of the strong coupling for protons at low fields, they can exhibit properties of long-lived spin states (LLSS).[213] For instance, measurements at 0.05 T for propane gas gave $T_{LLSS}/T_1 \approx 3.1$ at 3−7.6 bar, with $T_1 \approx 4$ s and $T_{LLSS} \approx 13$ s at 7.6 bar.[214] Similar trends were reported for diethyl ether vapor.[215] The spin-lock induced crossing (SLIC) pulse sequence can be conveniently used to convert LLSS to an observable signal.[214,215] Another challenge with heterogeneous hydrogenation is that it is outperformed by its homogeneous counterpart in the polarization levels achieved due to low selectivity to pairwise H_2 addition, often $P_{1H} = 1-3\%$ or even lower. Values of $P_{1H} = 7-10\%$[205,216−218] or even 60%[219] have been reported using heterogeneous catalysis but in most cases accompanied by low levels of catalytic conversion.

PURIFICATION

As soon as the development of PHIP as a hyperpolarization method for metabolic MRI began,[5,139] it became apparent that purification of the reaction solution would be necessary for preclinical and clinical *in vivo* applications. In this regard, PHIP presents some challenges. As outlined above, the hyperpolarization often requires rather nonphysiological conditions (organic solvents, pH value, temperature) and high concentrations of organometallic catalysts.[5,13,19,24,89,90,129,130,139,151] Moreover, the hydrogenation reaction may be incomplete or lead to side products.[24] Hence, purifying the polarized solution is important and, keeping in mind the short lifetime of liquid-state hyperpolarization, needs to be performed as quickly as possible, ideally within a few tens of seconds. Many purification strategies exist in chemistry already and some were adapted to PHIP as described below.

Catalyst Scavenging. One way to remove the catalyst is metal scavenging. In this approach, the scavenger is either used in a filtration column or mixed with the reaction solution and subsequently filtered out.[81,115,139,220] A commercially available metal scavenger (QuadraPure TU) was employed to clean a solution of HP fumarate prior to *in vivo* MRI.[115] Near complete removal of ruthenium was achieved by slowly passing the solution through the scavenger in about a minute, but a reduction of concentration from ~7 g/L to 100 mg/L was reached within seconds.[115] Similar scavenging approaches have

https://doi.org/10.1021/acs.analchem.1c04863
Anal. Chem. 2022, 94, 479−502

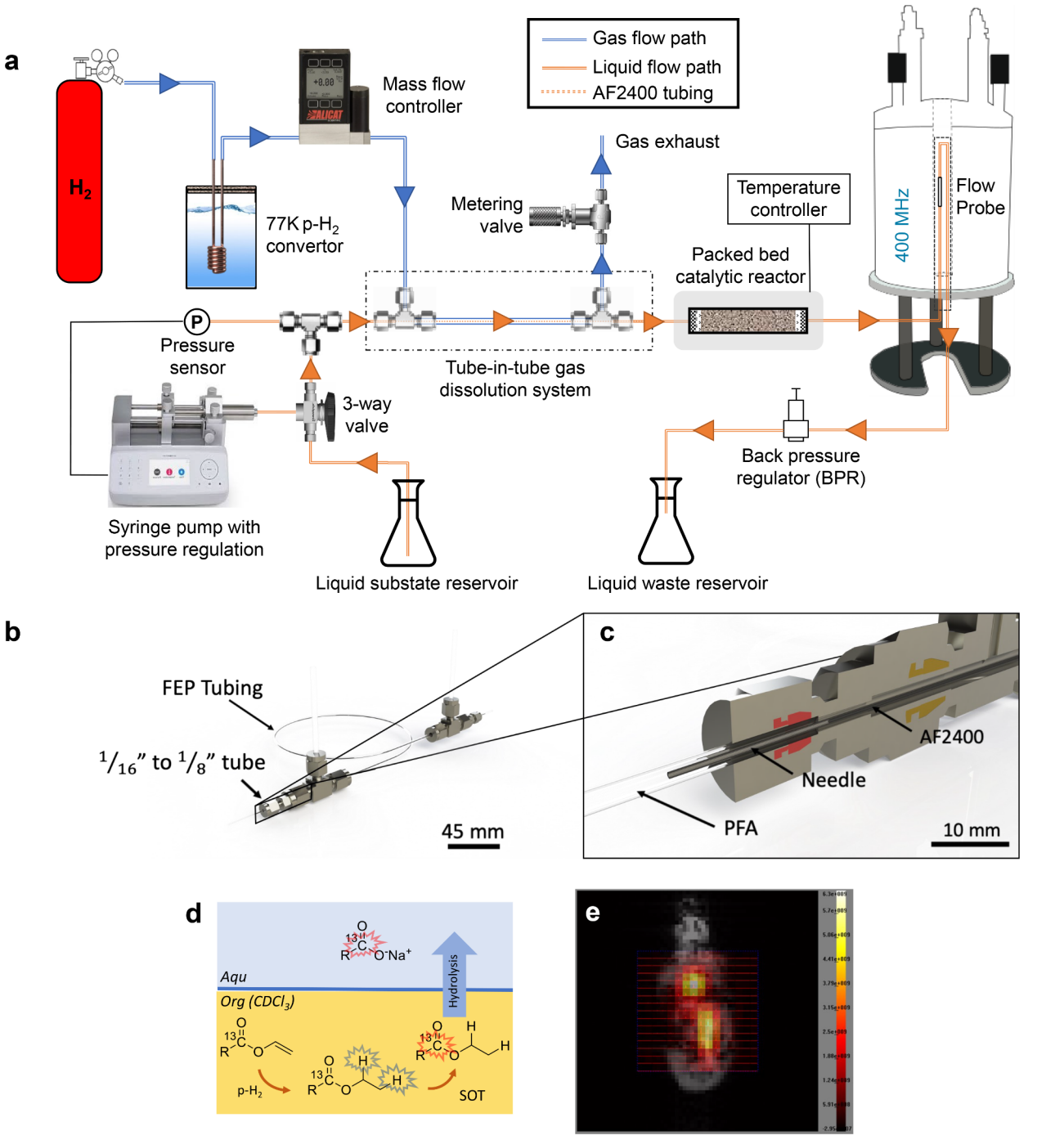

Figure 7. Upper panel: Continuous-flow liquid-state ALTADENA HET-PHIP polarizer. (a) The system incorporated a packed-bed heterogeneous reactor containing a solid Rh/TiO_2 nanorod catalyst and a tube-in-tube membrane system for bubble-free pH_2 dissolution. The liquid is drawn into the syringe from the left liquid reservoir and the 3-way valve is then changed to allow the liquid to flow through the tube-in-tube and then on to the heated catalyst cartridge. (b) Rendering of the tube-in-tube device. (c) Close up of the liquid inlet port showing the PFA (clear) tubing, 316 stainless steel needle (gray), and AF2400 membrane "inner tube" (black). Figure reproduced from Toward Continuous-Flow Hyperpolarisation of Metabolites via Heterogenous Catalysis, Side-Arm-Hydrogenation, and Membrane Dissolution of Parahydrogen, Hale, W. G.; Zhao, T. Y.; Choi, D.; Ferrer, M.-J.; Song, B.; Zhao, H.; Hagelin-Weaver, H. E.; Bowers, C. R. *ChemPhysChem*, Vol. *22*, Issue 9, 822−827 (ref 17). Copyright 2021 Wiley. Lower panel: PHIP-SAH LL-separation (left) and HP *in vivo* ^{13}C-MRI (right). The scheme on the left shows the LL separation of a carboxylate sodium salt in the water phase from its ester in the organic phase. HP [1-^{13}C]pyruvate obtained using this method has been applied *in vivo* for metabolic studies (right): ^{13}C-CSI image of [1-^{13}C]pyruvate overlaid with an anatomical image (^{1}H-RARE) of a healthy mouse (image acquired at 3 T).

been introduced by Kidd et al.[220] and Barskiy et al.[81] to remove an iridium-based SABRE catalyst.

A shortcoming of metal scavenging is that although the catalyst is removed, unreacted starting materials and side products may remain. Nevertheless, it was found to be a useful step for reducing the remaining metal contamination further in already purified solutions.[81]

https://doi.org/10.1021/acs.analchem.1c04863
Anal. Chem. 2022, 94, 479−502

Liquid−Liquid Phase Separation. Liquid−liquid (LL) phase extraction was found to provide near catalyst-free aqueous solutions of PHIP contrast agents. This method relies on the following steps: (a) hydrogenation of a labile, lipophilic precursor of the target substrate in a hydrophobic organic solvent (*e.g.*, chloroform); (b) SOT; (c) hydrolysis of the hyperpolarized product by means of fast reaction with an aqueous base, for instance, carboxylate sodium salts (hydrophilic) can be obtained by hydrolysis of the corresponding esters (lipophilic); and (d) extraction of the aqueous phase that contains the hydrophilic product, Figure 7.[79] To obtain a biocompatible pH, an acidic buffer was added.[56,80,82,221] The technique was shown to work well with PHIP-SAH[19] and has provided aqueous solution of hyperpolarized sodium [1-^{13}C]-pyruvate and acetate, *e.g.*, by hydrogenating their propargylic or vinyl esters.

The LL phase extraction can be performed in any solvent-resistant container, *e.g.*, in NMR tubes or a dedicated reactor. Its efficiency depends on the level of dispersion of small droplets of the organic solution into the aqueous phase, as hydrolysis likely occurs at the LL interface. As the dispersion should happen as fast as possible, injecting heated and pressurized base solution into the organic phase was suggested (a video showing the procedure can be found in ref 222). Instead of using pure hydrophobic chloroform,[223] mixtures containing some (a few %) hydrophilic solvents (*i.e.*, ethanol, methanol) or toluene have been suggested[82,222] to further improve the LL mixing and hydrolysis as well as bubbling N_2 gas through the solution.[82] Ultimately, thanks to the instability of the LL mixture, the two phases separate within a few seconds.

Notably, this approach was used for the first *in cellulo* and *in vivo* metabolic studies with PHIP-polarized pyruvate,[80,221,223] after a first demonstration of hyperpolarized [1-^{13}C]succinate (from maleic anhydride).[79] Losses of polarization during hydrolysis and phase transfer of the ester derivatives have been observed and could not be explained by T_1 relaxation alone.[159] Instead, the effect has been attributed to the presence of paramagnetic impurities derived from catalyst degradation in the organic phase, and a beneficial effect on hyperpolarization has been obtained through the addition of a radical scavenger (sodium ascorbate) to the aqueous base. The concentration of the metal (rhodium) in the aqueous phase has been determined to be 30 μM.[224]

Solvents such as methanol, ethanol, and acetone mix well with water and are transferred to the aqueous phase during phase extraction. Therefore, their application in the hyperpolarization of substrates for biological use (in cells and *in vivo*) must be considered carefully, due to their toxicity, especially for methanol. Nevertheless, it must be mentioned that, even when pure hydrophobic solvents (chloroform and toluene) were used, their dissolution and ultimately the concentration in the aqueous phase is non-negligible and a cytotoxicity effect has been observed.[221] In order to solve this issue, filtration of the aqueous solution through a lipophilic resin (Tenax TA, Porous Polymer Adsorbent, 60−80 mesh, Supelco) was recently shown to lead to a reduction of the concentration of these solvents well below the concentration recommended by the Environmental Protection Agency (EPA).[69,222]

Heterogeneous Catalysts. In contrast to homogeneous catalysis, heterogeneous catalysis affords straightforward separation of the solution-state hyperpolarized hydrogenation products from the solid catalyst due to the insolubility of the latter. Moreover, heterogeneous catalysis is inherently compatible with continuous-flow production of HP gases and liquids. These advantages were already recognized in the initial demonstration of HET-PHIP[73] and continue to drive the development of HET-PHIP catalysts and reactor systems.

In ref 73, silica and a polymer were functionalized with phosphine groups to tether the Rh complex (*e.g.*, Wilkinson's catalyst). The linkage proved to be resilient, but the catalysts still suffered from low stability, with possible leaching into solution upon oxidation of the phosphine moieties, reduction during the reaction, and metal complex dimerization.[194] A recent article described an alternative linkage scheme, where a silica-supported polymer incorporating pyridyl groups was used to tether Wilkinson's catalyst.[225] This catalyst showed better stability and resistance to leaching. Modest signal enhancements of up to 200 were reported for the hydrogenation of styrene in acetone-d_6.

In the quest to realize efficient, stable, and robust HET-PHIP catalysts, metal-oxide-supported nanoparticle catalysts consisting of Pt, Pd, Rh, Ru, Ir as well as bimetallic compositions (*e.g.*, Pd−In)[226] and intermetallic nanoparticles (*e.g.*, PtSn, Pt_3Sn)[216] with varying shapes, sizes, and support materials have been explored.[194] Most of the published solution-state HET-PHIP studies were performed using a batch reactor configuration,[216,226−229] where hydrogen is bubbled through a heated NMR tube containing the insoluble solid catalyst and the unsaturated substrate in solution. For larger catalyst particles (millimeter size), settling out of the catalyst after cessation of bubbling can occur within seconds. Under the relatively mild conditions of solution-state hydrogenation, supported metal nanoparticles were found to resist leaching. For example, after hydrogenation of 2-hydroxyethyl acrylate over 25 mg of Pt_3Sn intermetallic nanoparticles in 2 mL of D_2O at 120 °C and 5.7 bar, Pt and Sn levels in the decanted solution were found to be well below 100 ppb (by mass).[216] Transfer of hyperpolarization to heteronuclei in aqueous media for biologically relevant compounds has been addressed as well.[230]

As noted above, MRI of HP ^{13}C pyruvate provides a means for detection of abnormal metabolism in malignant tumors and other pathologies. There is evidence, however, that administration of a continuous stream of the HP pyruvate over longer periods is preferable to a single large bolus for some applications.[231] Production of purified continuous-flow streams of HP pyruvate by either dissolution DNP or PHIP is challenging and has not yet been demonstrated.

Hale et al. recently presented a novel apparatus that allowed continuous production of hyperpolarized allyl acetate by hydrogenation of propargyl acetate with pH_2, Figure 7. The apparatus incorporated a packed-bed catalytic reactor, side arm hydrogenation, and pH_2 membrane dissolution.[17] The polarizer continuously achieved a conversion of 30% and ^{1}H signal enhancements up to 300 (relative to thermal equilibrium at 9.4 T) were shown to be feasible. However, the polarization transfer to ^{13}C, side arm cleavage, and transfer to the aqueous phase have yet to be demonstrated.

Challenges for heterogeneous catalysis include lower product concentrations and lower polarizations compared to homogeneous approaches. To solve these shortcomings, emphasis is made on improved flow reactor design as well as the rational design of catalysts to obtain higher pairwise selectivity without sacrificing yield.

https://doi.org/10.1021/acs.analchem.1c04863
Anal. Chem. 2022, 94, 479−502

Precipitation. Very recently, a scheme to purify HP molecules based on precipitation was introduced.[24,232] HP fumarate was generated in an aqueous solution using a trans-selective hydrogenation catalyst. After hydrogenation and polarization transfer, the reaction solution contained the ruthenium-based catalyst, unreacted starting material, and side products in addition to the desired HP fumarate salt. To purify the solution, acid and nonpolarized fumarate were added to the solution so that fumaric acid precipitated out of the solution almost immediately.

Because fumarate precipitated very efficiently and the catalyst, starting material, and side products remained mostly dissolved, separation was easily achieved by decanting the solution. Subsequently, the solid, HP fumaric acid was redissolved in aqueous solution. It was important to keep the solid fumarate (from precipitation to redissolution) at a sufficiently high magnetic field to avoid fast relaxation in the solid state. The remaining metal concentration was found to be 16 μM after a washing procedure.[24] While this method worked well for fumarate, the generality of this approach remains an open question, and further research toward this promising approach is certainly warranted.

OTHER PROMISING DEVELOPMENTS

PHIP-on-a-Chip. An emerging research area that is mainly pursued at high magnetic fields is the integration of PHIP into lab-on-a-chip devices.[17,233−236] The advantage offered by working at a microfluidic scale (*i.e.*, with sample volumes on the order of microliters) is in the much higher degree of experimental control that can be leveraged, in terms of sample contact time with pH_2, molecular diffusion, temperature, and pressure. The other important benefit of microfluidic implementation of PHIP experiments is the short transport paths (and hence time) between the point of the PHIP process occurring and signal detection. This is particularly important when nuclear spin relaxation times are short.

Radio Amplification by Stimulated Emission of Radiation (RASER). RASER using PHIP was recently discovered[20,237] in PASADENA and ALTADENA conditions.[21,238] RASER emission was detected at low (millitesla)[237] and high fields (tesla) and reproduced by simulations.[21,23] Although the RASER effect was first observed using other HP techniques,[239−241] PHIP has the advantage that the polarization can be continuously refreshed by a constant supply of pH_2 as long as substrate is not depleted. While a biomedical application of RASER was not described, newly emerged applications included observation of NMR spectra with very narrow signals,[21,237] background-free proton NMR spectroscopy,[238] and polarization transfer to other molecules via intermolecular dipole−dipole interaction.[22]

PHIP-X. PHIP relayed via proton exchange (PHIP-X)[26] enables polarization of molecules that participate in proton exchange like glucose.[25,242−244] First, pH_2 is added to an intermediary molecule by homogeneous catalysis, where the polarization is then transferred to an exchanging proton. Second, the polarization is incorporated by the target molecule by exchange of a polarized proton from the reacted intermediary molecule. Experimentally, this process was implemented by placing a high-pressure reaction chamber in millitesla fields. Upon hydrogenation, the sample was transferred to high-field NMR for detection. If necessary, the target molecule can be added after the hydrogenation to avoid interference with the hydrogenation step. Both millitesla and MFC setups appear to be well suited to host this process, which involves SOT in the intermediary and target molecule, for which the spin physics has yet to be fully elucidated.

TOWARD CLINICAL APPLICATION

The results described above impressively demonstrate the power, versatility, and maturity of pH_2-based hyperpolarization approaches and instrumentation. Indeed, HP [1-^{13}C]pyruvate produced by hydrogenative PHIP has been recently employed to detect the response of the heart to altered metabolism in real time (Figure 8).[80]

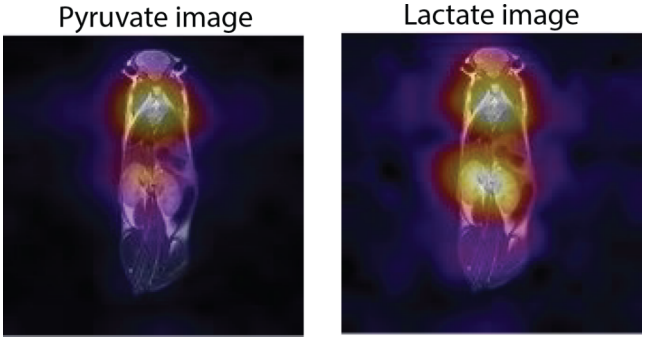

Figure 8. ^{13}C-chemical shift imaging reporting of pyruvate and lactate distribution acquired on living mice, obtained upon the injection of a dose of [1-^{13}C] pyruvate hyperpolarized using pH_2. The spatial localization of each metabolite is shown upon overlapping the ^{13}C-CSI results to the anatomical proton image (T_2 weighted fast spin echo image). Each metabolite map is scaled individually and is displayed on a fire color scale so that the region of highest metabolite signal appears white and the lowest appears black. Reprinted by permission from Nature: Sci. Rep., The 13C hyperpolarized pyruvate generated by ParaHydrogen detects the response of the heart to altered metabolism in real time, Cavallari, E.; Carrera, C.; Sorge, M.; Bonne, G.; Muchir, A.; Aime, S.; Reineri, F., *Sci. Rep.*, Vol. *8*, Issue 1, 8366 (ref 80). Copyright Nature 2018.

While preclinical imaging with PHIP agents was demonstrated in more than 15 papers since 2001, this method has not been translated to human imaging yet.[5,36,69,80,86,87,90,91,115,144−148,152]

Still, we may have reached a tipping point, as all ingredients for producing clean, aqueous solutions of interesting (not only biocompatible) agents were described in the literature. As we speak, work continues at multiple locations to make studies with PHIP-polarized agents a reality.

Let us assume that all relevant technical hurdles were addressed and that there was a device that produces a clean and pure solution or solid of highly polarized contrast agent with a fast and relevant function *in vivo*. Still, there will be regulatory aspects to meet before human studies may commence. Here, much can be learned from the path taken so impressively by the DNP community.

Contrast agents are considered drugs by most regulatory bodies. As no injectable HP contrast agents are approved as drugs (yet), the guidelines for the application and evaluation of nonapproved drugs apply. On the other hand, propane (also known as E944) is approved for unlimited use in foods and is already regulated by FDA. The above regulatory requirements may vary between countries but are likely to include:

1. GMP manufacturing of ingredients by vendor or in-house: pH_2, catalyst, solvents, precursors;

https://doi.org/10.1021/acs.analchem.1c04863
Anal. Chem. 2022, 94, 479−502

2. ISO 5 clean bench (or higher depending on regulations) preparation of ingredients on site: mixing precursor solution, pH_2;
3. Polarization and rapid QC: measure sample concentration, temperature, pH, and polarization; residual catalyst concentration; perform sterile filter integrity test.

These steps would be followed by transfer, administration by an MD or qualified person, and imaging. However, prior to injection, the hyperpolarized CA should be passed through a 0.2 μm pore size filter (the integrity of the filter would need to be tested in accordance with manufacturer regulations to ensure sterility). Given the limited lifetime of hyperpolarization, the QC needs to be rapid (<30 s) and is recommended to be performed in parallel with the sample transfer and filter integrity test to minimize the time to injection. The transfer distance will be determined by the lifetime, and long-lived samples may be transported between sites. Attempts for individual treatment of patients on a small scale may require less stringent regulations. Safety and dose escalation trials would be followed by efficacy tests.

CONCLUSIONS

pH_2-based hyperpolarization has come a long way since its inception in the 1980s, and the first demonstration of hyperpolarized *in vivo* ^{13}C-MRI in 2001. For hyperpolarizing small molecules in solution for *in vivo* MRI application, dDNP is currently the state-of-the-art methodology, but PHIP is beginning to emerge as a viable alternative. Arguably, there is no hyperpolarization technique that is more flexible and that offers more variants than PHIP. Consequently, many applications have emerged, ranging from basic physics to chemistry and biomedicine. The latter, however, has not advanced as fast as, *e.g.*, with dDNP.

The main advantages of PHIP lie in the inherent low cost, ease of implementation, rate of hyperpolarized sample turnover, and scalability. These advantages stem mainly from the chemical nature of the technique; hyperpolarization is delivered via chemical reactions rather than requiring cryogenic cooling of the to-be-polarized substance and/or irradiation with high power microwaves, as is the case for dDNP. The chemical basis of the process unfortunately carries some drawbacks: (1) the method is limited to polarizing molecules that can be generated through hydrogenation reactions; (2) the HP solutions are contaminated with other chemicals from the reaction; and (3) polarization levels are often only modest since the nuclear spins relax during the hyperpolarization process.

All three drawbacks are being overcome through state-of-the-art research, much of which is covered in this review: Many biologically and diagnostically promising agents are available by direct hydrogenation (SUX, FUM, TFPP, PLAC) and variants such as PHIP-SAH and PHIP-X (pyruvate, acetate, glucose, lactate). Physicochemical methods for purifying the HP solutions through phase separation have been shown for a few PHIP-polarized metabolites, and scavenging can be used to remove the catalyst from solutions. Advances in instrumentation for hydrogenation, polarization transfer, and sample transport, have helped to improve the resulting polarization levels in PHIP-polarized molecules. PHIP seems to be a promising hyperpolarization method for preclinical MRI and *in vitro* studies where experiment turnover is high but requirements for high polarization and solution sterility/nontoxicity are lower.

Nonetheless, it remains to be seen whether PHIP has a future role to play in clinical imaging. To date, no device is commercially available, not even for *in vitro* and preclinical *in vivo* studies. Over the years, some initiatives were and still are active (Amersham, Stelar, Spindynamics, Bruker, XEUS Technologies LTD, NVision), and numerous patents were filed. The technical challenges toward clinical applications are accompanied by regulatory aspects, which must be met for use in humans. Here, the contrast agents do not only need to be pure and highly polarized but also produced effectively and compliant to GMP. The reactive nature of PHIP may pose a challenge, too. Ideally, agents must have a long-enough lifetime for testing and transport after polarization.

Although the focus of this review has largely been on producing PHIP-polarized biomolecules for *in vivo* applications, there are many more uses of PHIP. Examples include studying chemical reaction mechanisms and as a source of signal enhancement for high-resolution NMR. Advances in instrumentation have underpinned much of the method development made in recent years and will continue to pave the way into the future. Even if PHIP (or hyperpolarization in general) would eventually turn out to be ineligible for clinics, many more applications are lurking behind the corner; the marriage of pH_2 and MR are far from over yet, and the best is yet to come.

AUTHOR INFORMATION

Corresponding Authors

Andreas B. Schmidt − *Department of Radiology−Medical Physics, Medical Center, Faculty of Medicine, University of Freiburg, Freiburg 79106, Germany; German Cancer Consortium (DKTK), partner site Freiburg and German Cancer Research Center (DKFZ), Heidelberg 69120, Germany;* orcid.org/0000-0001-8944-7463; Email: andreas.schmidt@uniklinik-freiburg.de

Jan-Bernd Hövener − *Section Biomedical Imaging, Molecular Imaging North Competence Center (MOIN CC), Department of Radiology and Neuroradiology, University Medical Center Kiel, Kiel University, 24118 Kiel, Germany;* orcid.org/0000-0001-7255-7252; Email: jan.hoevener@rad.uni-kiel.de

Authors

C. Russell Bowers − *Department of Chemistry, University of Florida, Gainesville, Florida 32611, United States; National High Magnetic Field Laboratory, Tallahassee, Florida 32310, United States*

Kai Buckenmaier − *High-Field Magnetic Resonance Center, Max Planck Institute for Biological Cybernetics, 72076 Tübingen, Germany*

Eduard Y. Chekmenev − *Intergrative Biosciences (Ibio), Department of Chemistry, Karmanos Cancer Institute (KCI), Wayne State University, Detroit, Michigan 48202, United States; Russian Academy of Sciences (RAS), 119991 Moscow, Russia;* orcid.org/0000-0002-8745-8801

Henri de Maissin − *Department of Radiology−Medical Physics, Medical Center, Faculty of Medicine, University of Freiburg, Freiburg 79106, Germany; German Cancer Consortium (DKTK), partner site Freiburg and German Cancer Research Center (DKFZ), Heidelberg 69120, Germany*

James Eills − *Institute for Physics, Johannes Gutenberg University, D-55090 Mainz, Germany; GSI*

https://doi.org/10.1021/acs.analchem.1c04863
Anal. Chem. 2022, 94, 479−502

Helmholtzzentrum für Schwerionenforschung GmbH, Helmholtz-Institut Mainz, 55128 Mainz, Germany; orcid.org/0000-0001-8468-6860

Frowin Ellermann − *Section Biomedical Imaging, Molecular Imaging North Competence Center (MOIN CC), Department of Radiology and Neuroradiology, University Medical Center Kiel, Kiel University, 24118 Kiel, Germany;* orcid.org/0000-0001-6446-6641

Stefan Glöggler − *NMR Signal Enhancement Group Max Planck Institutefor Biophysical Chemistry Am Fassberg 11, 37077 Göttingen, Germany; Center for Biostructural Imaging of Neurodegeneration of UMG, 37075 Göttingen, Germany*

Jeremy W. Gordon − *Department of Radiology & Biomedical Imaging, University of California San Francisco, San Francisco, California 94158, United States*

Stephan Knecht − *NVision Imaging Technologies GmbH, 89081 Ulm, Germany*

Igor V. Koptyug − *International Tomography Center, Siberian Branch of the Russian Academy of Sciences (SB RAS), Novosibirsk 630090, Russia;* orcid.org/0000-0003-3480-7649

Jule Kuhn − *Section Biomedical Imaging, Molecular Imaging North Competence Center (MOIN CC), Department of Radiology and Neuroradiology, University Medical Center Kiel, Kiel University, 24118 Kiel, Germany*

Andrey N. Pravdivtsev − *Section Biomedical Imaging, Molecular Imaging North Competence Center (MOIN CC), Department of Radiology and Neuroradiology, University Medical Center Kiel, Kiel University, 24118 Kiel, Germany*

Francesca Reineri − *Department of Molecular Biotechnology and Health Sciences, University of Torino, 10124 Torino, Italy*

Thomas Theis − *Departments of Chemistry, Physics, and Biomedical Engineering, North Carolina State University, Raleigh, North Carolina 27695, United States;* orcid.org/0000-0001-6779-9978

Kolja Them − *Section Biomedical Imaging, Molecular Imaging North Competence Center (MOIN CC), Department of Radiology and Neuroradiology, University Medical Center Kiel, Kiel University, 24118 Kiel, Germany;* orcid.org/0000-0002-5512-0910

Complete contact information is available at: https://pubs.acs.org/10.1021/acs.analchem.1c04863

Author Contributions

The manuscript was written through contributions of all authors. All authors have given approval to the final version of the manuscript.

Notes

The authors declare the following competing financial interest(s): E.Y.C. has a stake of ownership in XeUS Technologies LTD. S.K. is employed at NVision Imaging GMBH Ulm, Germany. T.T. holds stock in Vizma Life Sciences LLC (VLS) and is President of VLS. The terms of this arrangement have been reviewed and approved by NC State University in accordance with its policy on objectivity in research. XeUS Technologies LTD, NVision Imaging GMBH, and VLS are developing products related to the research being reported. All other authors declare no competing interests.

Biographies

Andreas B. Schmidt studied physics at the University of Freiburg (Germany) and Complutense Madrid (Spain) and received his Diploma and Ph.D. from University of Freiburg in 2015 and 2020, respectively. He became a Postdoctoral Researcher at the University Medical Center Freiburg (Germany) where he took over the lead of the hyperpolarization group shortly after. Since 2021, Andreas is also affiliated with the German Cancer Consortium (DKTK) and German Cancer Research Center (DKFZ, Heidelberg, Germany) as principal investigator. His research activities focus on PHIP and nuclear spin singlet states for biomedical applications.

C. Russell Bowers received his B.A. degree in 1985 from Bowdoin College, Brunswick, ME, and a Ph.D. in Chemical Physics in 1990 with Daniel P. Weitekamp at the California Institute of Technology, Pasadena, CA. As a NATO-NSF Postdoctoral Fellow, Bowers spent a year in the lab of Michael Mehring at the 2nd Physics Institute, University of Stuttgart (Germany). From 1992 to 1993, he was a Postdoc with Alexander Pines at the University of California, Berkeley, and Lawrence Berkeley Laboratory. Bowers joined the faculty at the University of Florida, Gainesville, FL, in January 1994 where he is currently a Full Professor of Chemistry and an affiliate of the National High Magnetic Field Laboratory. Bowers has contributed to the development of multiple NMR hyperpolarization techniques with a recent focus on parahydrogen enhanced NMR by heterogeneous catalysis.

Kai Buckenmaier studied physics at the University of Tübingen (Germany), where he received his diploma and Ph.D. degrees in 2006 and 2010, respectively. He worked for 1 year as a Postdoctoral Researcher in the Department of Experimental Physics at the University of Tübingen (Germany) and for 2 years in the Physics Department at the University of California in Berkeley, CA. Since 2013, he has been a Researcher at the Magnetic Resonance Center of the Max Planck Institute for Biological Cybernetics, Germany. His current research activities include the development and implementation of different hyperpolarization methods for ultralow-field magnetic resonance imaging.

Eduard Y. Chekmenev earned his Ph.D. in Physical Chemistry in 2003 (supervisor Prof. Richard J. Wittebort), University of Louisville, KY. He studied as a Postdoctoral Fellow at the NHMFL in Tallahassee, FL (supervisor Prof. Timothy Cross), at Caltech (supervisor Prof. Daniel P. Weitekamp), and at HMRI (supervisor Dr. Brian D. Ross). In 2009, Dr. Chekmenev started his hyperpolarization program at Vanderbilt University Medical Center, where he was tenured in 2015. In 2018, Eduard moved to the Department of Chemistry and Karmanos Cancer Institute (KCI) at Wayne State University in Detroit, MI, to continue his research on MR hyperpolarization. His research interests include development of methods of hyperpolarization using parahydrogen induced polarization and spin exchange optical pumping and biomedical imaging and industrial use of NMR hyperpolarization techniques.

Henri de Maissin graduated from the Institut d'Optique Graduate School in Paris (France) in 2016, then studied biomedical technologies at the University of Tübingen (Germany) where he obtained his Master's Degree in 2021. For his Master's thesis, he worked at the University Medical Center Freiburg (Germany) on the topic "Effective spin order transfer at high field in an MRI system". He is now pursuing his Ph.D. in the same group in Freiburg. His research projects include *in situ* PHIP in MRI systems (SAMBADENA) and sequence development for ^{13}C imaging of hyperpolarized agents.

James Eills studied Chemistry at the University of Southampton (U.K.) from 2011 to 2015, doing his Master's research in that time at UC Berkeley, CA. During his Ph.D., he worked on hyperpolarization techniques for NMR and microfluidic engineering, earning his Ph.D. from the University of Southampton in 2019. He then moved to

Johannes Gutenberg University Mainz to work at the Helmholtz Institute as a Postdoctoral Research Fellow to develop zero- to ultralow-field NMR techniques, a unique type of NMR experiment performed in the absence of a magnetic field.

Frowin Ellermann studied Materials Science and Engineering at the University of Kiel (Germany), where he received his Bachelor's Degree in 2015 and his Master's Degree in 2018, respectively. After graduation, he worked as a Fellow in the Collaborative Research Center 1261 "Magnetoelectric Sensors" (German Research Foundation). Since 2019, he has been a Doctoral Candidate in hyperpolarization at the Section Biomedical Imaging at the University Medical Center Schleswig-Holstein, Kiel (Germany). As a part of the Research Training Group 2154 "Materials for Brain" (German Research Foundation), his current research activities include the development of contrast agents for metabolic MRI with a focus on instrumentation for parahydrogen-based hyperpolarization.

Stefan Glöggler obtained his Ph.D. from RWTH Aachen University (Germany) in 2013. He pursed Postdoctoral studies at UCLA in Los Angeles, CA, Université Bordeaux (France), and the University of Southampton (U.K.). In 2017, he started as an independent group leader at the Max-Planck Institute for Biophysical Chemistry in Göttingen (Germany) and is currently head of the Magnetic Resonance Signal Enhancement Lab. His research interests include the advancement of methods based on spin phenomena to answer biochemical and biological questions.

Jeremy W. Gordon earned his B.S. from the University of Georgia in Physics & Astronomy and received his Ph.D. from the University of Wisconsin-Madison in Medical Physics. He is currently an Assistant Professor in the Department of Radiology & Biomedical Imaging at UC San Francisco. His research focuses on the development of novel acquisition and reconstruction methods for quantitative imaging of cellular metabolism and the clinical translation of hyperpolarized ^{13}C MRI to provide unique metabolic characterization of organ function, disease staging, and response to therapy.

Stephan Knecht started his studies of Physics at the University of Tuebingen in 2006 and continued them at the University of Freiburg in 2008 (both Germany), where he received his Diploma and Ph.D. in Physics in 2014 and 2019, respectively. From 2018 to 2020, he joined the Physical Chemistry Department of the Technical University Darmstadt (Germany) as a Research Fellow. Since 2020, he has been the Associate Director of MR development at NVision Imaging Technologies GmbH Ulm, Germany.

Igor V. Koptyug studied Physics at the Novosibirsk State University, where he received his Diploma in Chemical Physics in 1985. He then became a Junior Researcher at the Institute of Chemical Kinetics and Combustion and received his Ph.D. Degree in 1991 there. In 1992−1995, he worked as a Postdoctoral Researcher in the Photochemistry Group of Prof. N. J. Turro (Columbia University, New York). Since 1995, he's been working at the International Tomography Center, Siberian Branch of the Russian Academy of Sciences in various capacities, where he currently holds positions of Head of Research, Chief Research Scientist, and a Research Group Leader, along with a part-time position at the Boreskov Institute of Catalysis, SB RAS. He earned his Dr. Sci. (Habilitation) Degree in Catalysis in 2003 and the title of Professor in 2006. His research interests include signal enhancement in NMR and applications of NMR and MRI in catalysis research.

Jule Kuhn received her Bachelor's Degree in Physics from the Institute of Physics at Kiel University (Germany) in 2019. She is currently a Master's student in the Section Biomedical Imaging at the University Medical Center Schleswig-Holstein, Germany. Her research is focused on PHIP of biological molecules as well as the development of experimental setups specialized for PHIP and PHIP-X.

Andrey N. Pravdivtsev received his Ph.D. in Chemical Physics at Novosibirsk State University and the International Tomography Center SB RAS (in the groups of Prof. K. L. Ivanov and Prof. A. V. Yurkovskaya) in 2017. From 2017 to 2019, he was a DAAD Fellow and later a Postdoctoral Researcher in the MRI and Hyperpolarization Group of Prof. J.-B. Hövener (Kiel University). Currently, he is a BMBF Juniorverbünde Fellow at Kiel University, where his research focuses on the development of PHIP and SABRE applications for *in vivo* MRI.

Francesca Reineri received her Master's and Ph.D. in Chemistry from University of Torino (Italy) in 1999 and 2002, respectively. Since 2008, she has been an Assistant Professor at the University of Torino, Department Molecular Biotechnology and Health Sciences, where she leads the Hyperpolarization Group at the Molecular Imaging Center. Her research focuses on the development of new hyperpolarized probes for imaging studies of cancer disease, development of cost-effective parahydrogen-based polarization methods, and diagnostic applications thereof.

Thomas Theis completed his undergraduate and Master's at the Georg-August University of Goettingen (Germany). He received his Ph.D. in 2012 from UC Berkeley, CA, working with Prof. Alexander Pines on "zero-field NMR" and "parahydrogen hyperpolarization schemes" for portable NMR. He conducted postdoctoral research at Duke University with Prof. Warren Warren that focused on "singlet states for hyperpolarization storage" and worked on "low-field NMR" as a Visiting Professor at RWTH Aachen University with Prof. Stephan Appelt (Germany). In 2015, he was promoted to Research Assistant Professor at Duke University developing "cost-efficient hyperpolarization techniques for molecular imaging". Since 2018, he leads the North Carolina State Hyperpolarization Laboratory. His research is focused on hyperpolarization technology and unconventional NMR and MRI detection schemes.

Kolja Them has studied Physics at the University of Hamburg, where he earned his diploma on Quantum Field Theory in Curved Space-Time. His Ph.D. was on the "C*-algebraic reformulation of Quantum Statistical Mechanics for the description of experimentally investigated spin systems". He was a Postdoc at the University-Medical Center Hamburg Eppendorf and worked on magnetic particle imaging. Now he is a Postdoc at the UKSH working on hyperpolarized MRI. He has more than 10 years of research experience in the field of spin systems.

Jan-Bernd Hövener studied Physics in Münster, Heidelberg, and Nice (France). After working in New York and in Pasadena, CA, he graduated in Physics at the University of Heidelberg in the group of Prof. P. Bachert. In 2009, he joined Prof. J. K. Hennig in Freiburg and was accepted to the Academy of Excellence in 2010 and the Emmy Noether Program of the DFG in 2014. In 2016, he received the Venia Legendi and Habilitation. In 2017, he became Professor for Translational MRI at Kiel University, where he heads the Section for Biomedical Imaging and the Molecular Imaging Competence Center North (MOIN CC). His research interests include novel imaging methods, focusing on conventional and hyperpolarized magnetic resonance imaging and spectroscopy.

■ ACKNOWLEDGMENTS

We acknowledge funding from German Federal Ministry of Education and Research (BMBF) within the framework of the e:Med Research and Funding Concept (Grant 01ZX1915C),

https://doi.org/10.1021/acs.analchem.1c04863
Anal. Chem. 2022, 94, 479−502

German Cancer Consortium (DKTK), DFG (Grants SCHM 3694/1-1, HO-4602/2-2, HO-4602/3, GRK2154-2019, EXC2167, FOR5042, SFB1479, and TRR287), Kiel University and the Faculty of Medicine, and Research Commission of the University Medical Center Freiburg (Grant SCHM2146-20), and support from the Core Facility Advanced Molecular Imaging Center (AMIR), Department of Radiology − Medical Physics of the University Hospital Freiburg. MOIN CC was founded by a grant from the European Regional Development Fund (ERDF) and the Zukunftsprogramm Wirtschaft of Schleswig-Holstein (Project No. 122-09-053), National Science Foundation (NSF) Grants CHE-2108306 and CBET-1933723, and the National High Magnetic Field Laboratory, which is supported by the NSF Cooperative Agreement No. DMR-1644779* and the State of Florida. This project has received funding from the European Union's Horizon 2020 Research and Innovation Programme under the Marie Skłodowska-Curie Grant Agreement No. 766402. T.T. acknowledges support from the National Institute of Biomedical Imaging and Bioengineering of the National Institutes of Health under Award Number NIH R01EB029829. E.Y.C thanks NSF CHE-1904780, DOD CDMRP W81XWH-20-10576, NIH NHLBI R21 HL154032. The content is solely the responsibility of the authors and does not necessarily represent the official views of the National Institutes of Health. I.V.K. acknowledges the Russian Ministry of Science and Higher Education (grant no. 075-15-2020-779) for financial support. The University of Torino was funded by the EU H2020 FETOPEN under the Grant Agreement No. 858149 (Alternatives to Gd). J.W.G. acknowledges support from the National Institutes of Health (Grant P41EB013598). We thank Dr. Mariya Pravdivtseva (UKSH, Kiel, Germany) for creating the TOC figure.

REFERENCES

(1) Born, M.; Heisenberg, W. *Ann. Phys.* **1924**, *379* (9), 1−31.
(2) Bowers, C. R.; Weitekamp, D. P. *Phys. Rev. Lett.* **1986**, *57* (21), 2645−2648.
(3) Bowers, C. R.; Weitekamp, D. P. *J. Am. Chem. Soc.* **1987**, *109* (18), 5541−5542.
(4) Eisenschmid, T. C.; Kirss, R. U.; Deutsch, P. P.; Hommeltoft, S. I.; Eisenberg, R.; Bargon, J.; Lawler, R. G.; Balch, A. L. *J. Am. Chem. Soc.* **1987**, *109* (26), 8089−8091.
(5) Golman, K.; Axelsson, O.; Johannesson, H.; Mansson, S.; Olofsson, C.; Petersson, J. S. *Magn. Reson. Med.* **2001**, *46* (1), 1−5.
(6) Johansson, E.; Olsson, L. E.; Månsson, S.; Petersson, J. S.; Golman, K.; Ståhlberg, F.; Wirestam, R. *Magn. Reson. Med.* **2004**, *52* (5), 1043−1051.
(7) Bargon, J.; Kandels, J.; Kating, P. *J. Chem. Phys.* **1993**, *98* (8), 6150−6153.
(8) Messerle, B. A.; Sleigh, C. J.; Partridge, M. G.; Duckett, S. B. *J. Chem. Soc., Dalton Trans.* **1999**, 1429−1436.
(9) Eills, J.; Stevanato, G.; Bengs, C.; Glöggler, S.; Elliott, S. J.; Alonso-Valdesueiro, J.; Pileio, G.; Levitt, M. H. *J. Magn. Reson.* **2017**, *274*, 163−172.
(10) Duckett, S. B.; Wood, N. J. *Coord. Chem. Rev.* **2008**, *252* (21), 2278−2291.
(11) Nelson, S. J.; Kurhanewicz, J.; Vigneron, D. B.; Larson, P. E. Z.; Harzstark, A. L.; Ferrone, M.; van Criekinge, M.; Chang, J. W.; Bok, R.; Park, I.; Reed, G.; Carvajal, L.; Small, E. J.; Munster, P.; Weinberg, V. K.; Ardenkjaer-Larsen, J. H.; Chen, A. P.; Hurd, R. E.; Odegardstuen, L.-I.; Robb, F. J.; Tropp, J.; Murray, J. A. *Sci. Transl. Med.* **2013**, *5* (198), 108.
(12) Ardenkjær-Larsen, J. H.; Bowen, S.; Petersen, J. R.; Rybalko, O.; Vinding, M. S.; Ullisch, M.; Nielsen, N. C. *Magn. Reson. Med.* **2019**, *81* (3), 2184−2194.
(13) Adams, R. W.; Aguilar, J. A.; Atkinson, K. D.; Cowley, M. J.; Elliott, P. I. P.; Duckett, S. B.; Green, G. G. R.; Khazal, I. G.; López-Serrano, J.; Williamson, D. C. *Science* **2009**, *323* (5922), 1708−1711.
(14) Barskiy, D. A.; Coffey, A. M.; Nikolaou, P.; Mikhaylov, D. M.; Goodson, B. M.; Branca, R. T.; Lu, G. J.; Shapiro, M. G.; Telkki, V.-V.; Zhivonitko, V. V.; Koptyug, I. V.; Salnikov, O. G.; Kovtunov, K. V.; Bukhtiyarov, V. I.; Rosen, M. S.; Barlow, M. J.; Safavi, S.; Hall, I. P.; Schröder, L.; Chekmenev, E. Y. *Chem. - Eur. J.* **2017**, *23* (4), 725−751.
(15) Kovtunov, K. V.; Koptyug, I. V.; Fekete, M.; Duckett, S. B.; Theis, T.; Joalland, B.; Chekmenev, E. Y. *Angew. Chem., Int. Ed.* **2020**, *59* (41), 17788−17797.
(16) Hövener, J.-B.; Schwaderlapp, N.; Lickert, T.; Duckett, S. B.; Mewis, R. E.; Highton, L. A. R.; Kenny, S. M.; Green, G. G. R.; Leibfritz, D.; Korvink, J. G.; Hennig, J.; von Elverfeldt, D. *Nat. Commun.* **2013**, *4*, 2946.
(17) Hale, W. G.; Zhao, T. Y.; Choi, D.; Ferrer, M.-J.; Song, B.; Zhao, H.; Hagelin-Weaver, H. E.; Bowers, C. R. *ChemPhysChem* **2021**, *22* (9), 822−827.
(18) Eshuis, N.; Aspers, R. L. E. G.; van Weerdenburg, B. J. A.; Feiters, M. C.; Rutjes, F. P. J. T.; Wijmenga, S. S.; Tessari, M. *Angew. Chem., Int. Ed.* **2015**, *54* (48), 14527−14530.
(19) Reineri, F.; Boi, T.; Aime, S. *Nat. Commun.* **2015**, *6*, 5858.
(20) Appelt, S.; Kentner, A.; Lehmkuhl, S.; Blümich, B. *Prog. Nucl. Magn. Reson. Spectrosc.* **2019**, *114*−*115*, 1−32.
(21) Pravdivtsev, A. N.; Sönnichsen, F. D.; Hövener, J.-B. *ChemPhysChem* **2020**, *21* (7), 667−672.
(22) Korchak, S.; Kaltschnee, L.; Dervisoglu, R.; Andreas, L.; Griesinger, C.; Glöggler, S. *Angew. Chem., Int. Ed.* **2021**, *60* (38), 20984−20990.
(23) Joalland, B.; Ariyasingha, N. M.; Lehmkuhl, S.; Theis, T.; Appelt, S.; Chekmenev, E. Y. *Angew. Chem., Int. Ed.* **2020**, *59* (22), 8654−8660.
(24) Knecht, S.; Blanchard, J. W.; Barskiy, D.; Cavallari, E.; Dagys, L.; Van Dyke, E.; Tsukanov, M.; Bliemel, B.; Munnemann, K.; Aime, S.; Reineri, F.; Levitt, M. H.; Buntkowsky, G.; Pines, A.; Blumler, P.; Budker, D.; Eills, J. *Proc. Natl. Acad. Sci. U. S. A.* **2021**, *118* (13), e2025383118.
(25) Roy, S. S.; Appleby, K. M.; Fear, E. J.; Duckett, S. B. *J. Phys. Chem. Lett.* **2018**, *9* (5), 1112−1117.
(26) Them, K.; Ellermann, F.; Pravdivtsev, A. N.; Salnikov, O. G.; Skovpin, I. V.; Koptyug, I. V.; Herges, R.; Hövener, J.-B. *J. Am. Chem. Soc.* **2021**, *143* (34), 13694−13700.
(27) Marshall, H.; Stewart, N. J.; Chan, H.-F.; Rao, M.; Norquay, G.; Wild, J. M. *Prog. Nucl. Magn. Reson. Spectrosc.* **2021**, *122*, 42−62.
(28) Hoevener, J.-B.; Bär, S.; Leupold, J.; Jenne, K.; Leibfritz, D.; Hennig, J.; Duckett, S. B.; von Elverfeldt, D. *NMR Biomed.* **2013**, *26*, 124−131.
(29) Feng, B.; Coffey, A. M.; Colon, R. D.; Chekmenev, E. Y.; Waddell, K. W. *J. Magn. Reson.* **2012**, *214*, 258−262.
(30) Wagner, S. *MAGMA* **2014**, *27* (3), 195−199.
(31) Aroulanda, C.; Starovoytova, L.; Canet, D. *J. Phys. Chem. A* **2007**, *111* (42), 10615−10624.
(32) Buntkowsky, G.; Walaszek, B.; Adamczyk, A.; Xu, Y.; Limbach, H.-H.; Chaudret, B. *Phys. Chem. Chem. Phys.* **2006**, *8* (16), 1929−1935.
(33) Schmidt, A. B.; Worner, J.; Pravdivtsev, A.; Knecht, S.; Scherer, H.; Weber, S.; Hennig, J.; Elverfeldt, D.; Hovener, J.-B. *ChemPhysChem* **2019**, *20* (19), 2408−2412.
(34) Kiryutin, A. S.; Sauer, G.; Yurkovskaya, A. V.; Limbach, H.-H.; Ivanov, K. L.; Buntkowsky, G. *J. Phys. Chem. C* **2017**, *121* (18), 9879−9888.
(35) Freeman, R.; Wittekoek, S.; Ernst, R. R. *J. Chem. Phys.* **1970**, *52* (3), 1529−1544.
(36) Kadlecek, S.; Vahdat, V.; Nakayama, T.; Ng, D.; Emami, K.; Rizi, R. *NMR Biomed.* **2011**, *24* (8), 933−942.

https://doi.org/10.1021/acs.analchem.1c04863
Anal. Chem. 2022, 94, 479−502

(37) Pravdivtsev, A. N.; Ivanov, K. L.; Kaptein, R.; Yurkovskaya, A. V. *Appl. Magn. Reson.* **2013**, *44* (1), 23−39.
(38) Schmidt, A. B.; Berner, S.; Schimpf, W.; Muller, C.; Lickert, T.; Schwaderlapp, N.; Knecht, S.; Skinner, J. G.; Dost, A.; Rovedo, P.; Hennig, J.; von Elverfeldt, D.; Hovener, J. -B. *Nat. Commun.* **2017**, *8*, 14535.
(39) Berner, S.; Schmidt, A. B.; Zimmermann, M.; Pravdivtsev, A. N.; Glöggler, S.; Hennig, J.; von Elverfeldt, D.; Hövener, J.-B. *ChemistryOpen* **2019**, *8* (6), 728−736.
(40) Natterer, J.; Bargon, J. *Prog. Nucl. Magn. Reson. Spectrosc.* **1997**, *31* (4), 293−315.
(41) Nasibulov, E. A.; Pravdivtsev, A. N.; Yurkovskaya, A. V.; Lukzen, N. N.; Vieth, H.-M.; Ivanov, K. L. *Z. Phys. Chem.* **2013**, *227* (6−7), 929−953.
(42) Goldman, M.; Johannesson, H. *C. R. Phys.* **2005**, *6*, 575−581.
(43) Torres, O.; Procacci, B.; Halse, M. E.; Adams, R. W.; Blazina, D.; Duckett, S. B.; Eguillor, B.; Green, R. A.; Perutz, R. N.; Williamson, D. C. *J. Am. Chem. Soc.* **2014**, *136* (28), 10124−10131.
(44) Pravdivtsev, A. N.; Yurkovskaya, A. V.; Petrov, P. A.; Vieth, H.-M. *Phys. Chem. Chem. Phys.* **2017**, *19* (38), 25961−25969.
(45) Bowers, C. R. *EMagRes* **2007**, DOI: 10.1002/9780470034590.emrstm0489.
(46) Bowers, C. R. *Parahydrogen and Synthesis Allow Dramatically Enhanced Nuclear Alignment*. Ph.D. Thesis, California Institute of Technology, Pasadena, CA, 1991; DOI: 10.7907/R5TV-Z220.
(47) Natterer, J.; Schedletzky, O.; Barkemeyer, J.; Bargon, J.; Glaser, S. J. *J. Magn. Reson.* **1998**, *133* (1), 92−97.
(48) Berner, S.; Schmidt, A. B.; Ellermann, F.; Korchak, S.; Chekmenev, E. Y.; Gloggler, S.; von Elverfeldt, D.; Hennig, J.; Hovener, J.-B. *Phys. Chem. Chem. Phys.* **2021**, *23* (3), 2320−2330.
(49) Pravica, M. G.; Weitekamp, D. P. *Chem. Phys. Lett.* **1988**, *145* (4), 255−258.
(50) Plaumann, M.; Bommerich, U.; Trantzschel, T.; Lego, D.; Dillenberger, S.; Sauer, G.; Bargon, J.; Buntkowsky, G.; Bernarding, J. *Chem. - Eur. J.* **2013**, *19* (20), 6334−6339.
(51) Bar, S.; Lange, T.; Leibfritz, D.; Hennig, J.; von Elverfeldt, D.; Hovener, J.-B. *J. Magn. Reson.* **2012**, *225*, 25−35.
(52) Svyatova, A.; Skovpin, I. V.; Chukanov, N. V.; Kovtunov, K. V.; Chekmenev, E. Y.; Pravdivtsev, A. N.; Hövener, J.-B.; Koptyug, I. V. *Chem. - Eur. J.* **2019**, *25* (36), 8465−8470.
(53) Shchepin, R. V.; Coffey, A. M.; Waddell, K. W.; Chekmenev, E. Y. *Anal. Chem.* **2014**, *86* (12), 5601−5605.
(54) Schmidt, A. B.; Brahms, A.; Ellermann, F.; Knecht, S.; Berner, S.; Hennig, J.; von Elverfeldt, D.; Herges, R.; Hovener, J.-B.; Pravdivtsev, A. *Phys. Chem. Chem. Phys.* **2021**, DOI: 10.1039/D1CP04153C.
(55) Jóhannesson, H.; Axelsson, O.; Karlsson, M. *C. R. Phys.* **2004**, *5* (3), 315−324.
(56) Cavallari, E.; Carrera, C.; Boi, T.; Aime, S.; Reineri, F. *J. Phys. Chem. B* **2015**, *119* (31), 10035−10041.
(57) Kadlecek, S.; Emami, K.; Ishii, M.; Rizi, R. *J. Magn. Reson.* **2010**, *205* (1), 9−13.
(58) Cai, C.; Coffey, A. M.; Shchepin, R. V.; Chekmenev, E. Y.; Waddell, K. W. *J. Phys. Chem. B* **2013**, *117* (5), 1219−1224.
(59) Duckett, S. B.; Newell, C. L.; Eisenberg, R. *J. Am. Chem. Soc.* **1993**, *115* (3), 1156−1157.
(60) Haake, M.; Natterer, J.; Bargon, J. *J. Am. Chem. Soc.* **1996**, *118* (36), 8688−8691.
(61) Stevanato, G. *J. Magn. Reson.* **2017**, *274*, 148−162.
(62) Korchak, S.; Yang, S.; Mamone, S.; Glöggler, S. *ChemistryOpen* **2018**, *7* (5), 344−348.
(63) Pravdivtsev, A. N.; Kozinenko, V. P.; Hövener, J.-B. *J. Phys. Chem. A* **2018**, *122* (45), 8948−8956.
(64) Stevanato, G.; Eills, J.; Bengs, C.; Pileio, G. *J. Magn. Reson.* **2017**, *277*, 169−178.
(65) Pravdivtsev, A. N.; Hövener, J.-B. *Phys. Chem. Chem. Phys.* **2020**, *22* (16), 8963−8972.
(66) Hogben, H. J.; Krzystyniak, M.; Charnock, G. T. P.; Hore, P. J.; Kuprov, I. *J. Magn. Reson.* **2011**, *208* (2), 179−194.
(67) Smith, S. A.; Levante, T. O.; Meier, B. H.; Ernst, R. R. *J. Magn. Reson., Ser. A* **1994**, *106* (1), 75−105.
(68) Bengs, C.; Levitt, M. H. *Magn. Reson. Chem.* **2018**, *56* (6), 374−414.
(69) Bhattacharya, P.; Harris, K.; Lin, A. P.; Mansson, M.; Norton, V. A.; Perman, W. H.; Weitekamp, D. P.; Ross, B. D. *MAGMA* **2005**, *18* (5), 245−256.
(70) Skovpin, I. V.; Zhivonitko, V. V.; Koptyug, I. V. *Appl. Magn. Reson.* **2011**, *41* (2), 393−410.
(71) Kovtunov, K. V.; Zhivonitko, V. V.; Corma, A.; Koptyug, I. V. *J. Phys. Chem. Lett.* **2010**, *1* (11), 1705−1708.
(72) Abdulhussain, S.; Breitzke, H.; Ratajczyk, T.; Grünberg, A.; Srour, M.; Arnaut, D.; Weidler, H.; Kunz, U.; Kleebe, H. J.; Bommerich, U.; Bernarding, J.; Gutmann, T.; Buntkowsky, G. *Chem. - Eur. J.* **2014**, *20* (4), 1159−1166.
(73) Koptyug, I. V.; Kovtunov, K. V.; Burt, S. R.; Anwar, M. S.; Hilty, C.; Han, S.-I.; Pines, A.; Sagdeev, R. Z. *J. Am. Chem. Soc.* **2007**, *129* (17), 5580−5586.
(74) Kovtunov, K. V.; Beck, I. E.; Bukhtiyarov, V. I.; Koptyug, I. V. *Angew. Chem., Int. Ed.* **2008**, *47* (8), 1492−1495.
(75) Glöggler, S.; Grunfeld, A. M.; Ertas, Y. N.; McCormick, J.; Wagner, S.; Schleker, P. P. M.; Bouchard, L.-S. *Angew. Chem., Int. Ed.* **2015**, *54* (8), 2452−2456.
(76) Kovtunov, K. V.; Barskiy, D. A.; Salnikov, O. G.; Shchepin, R. V.; Coffey, A. M.; Kovtunova, L. M.; Bukhtiyarov, V. I.; Koptyug, I. V.; Chekmenev, E. Y. *RSC Adv.* **2016**, *6* (74), 69728−69732.
(77) Kaltschnee, L.; Jagtap, A. P.; McCormick, J.; Wagner, S.; Bouchard, L.-S.; Utz, M.; Griesinger, C.; Glöggler, S. *Chem. - Eur. J.* **2019**, *25* (47), 11031−11035.
(78) Jagtap, A. P.; Kaltschnee, L.; Glöggler, S. *Chem. Sci.* **2019**, *10* (37), 8577−8582.
(79) Reineri, F.; Viale, A.; Ellena, S.; Boi, T.; Daniele, V.; Gobetto, R.; Aime, S. *Angew. Chem., Int. Ed.* **2011**, *50* (32), 7350−7353.
(80) Cavallari, E.; Carrera, C.; Sorge, M.; Bonne, G.; Muchir, A.; Aime, S.; Reineri, F. *Sci. Rep.* **2018**, *8* (1), 8366.
(81) Barskiy, D. A.; Ke, L. A.; Li, X.; Stevenson, V.; Widarman, N.; Zhang, H.; Truxal, A.; Pines, A. *J. Phys. Chem. Lett.* **2018**, *9* (11), 2721−2724.
(82) Dagys, L.; Jagtap, A. P.; Korchak, S.; Mamone, S.; Saul, P.; Levitt, M. H.; Glöggler, S. *Analyst* **2021**, *146* (5), 1772−1778.
(83) Goldman, M.; Johannesson, H.; Axelsson, O.; Karlsson, M. *C. R. Chim.* **2006**, *9*, 357−363.
(84) Goldman, M.; Axelsson, O.; Johannesson, H.; Ardenkjaer-Larsen, J. *Method and Apparatus for Producing Contrast Agents for Magnetic Resonance Imaging*. U.S. Patent Application 20060127313 A1, June 15, 2006.
(85) Waddell, K. W.; Coffey, A. M.; Chekmenev, E. Y. *J. Am. Chem. Soc.* **2011**, *133* (1), 97−101.
(86) Coffey, A. M.; Shchepin, R. V.; Truong, M. L.; Wilkens, K.; Pham, W.; Chekmenev, E. Y. *Anal. Chem.* **2016**, *88*, 8279−8288.
(87) Coffey, A. M.; Shchepin, R. V.; Feng, B.; Colon, R. D.; Wilkens, K.; Waddell, K. W.; Chekmenev, E. Y. *J. Magn. Reson.* **2017**, *284*, 115−124.
(88) Joalland, B.; Schmidt, A. B.; Kabir, M. S. H.; Chukanov, N. V.; Kovtunov, K. V.; Koptyug, I. V.; Hennig, J.; Hövener, J.-B.; Chekmenev, E. Y. *Anal. Chem.* **2020**, *92* (1), 1340−1345.
(89) Hövener, J.-B.; Chekmenev, E. Y.; Harris, K. C.; Perman, W. H.; Tran, T. T.; Ross, B. D.; Bhattacharya, P. *MAGMA* **2009**, *22*, 123−134.
(90) Hövener, J.-B.; Chekmenev, E. Y.; Harris, K. C.; Perman, W. H.; Robertson, L. W.; Ross, B. D.; Bhattacharya, P. *MAGMA* **2009**, *22*, 111−121.
(91) Schmidt, A. B.; Berner, S.; Braig, M.; Zimmermann, M.; Hennig, J.; von Elverfeldt, D.; Hovener, J.-B. *PLoS One* **2018**, *13* (7), No. e0200141.
(92) Agraz, J.; Grunfeld, A. M.; Cunningham, K.; Pozos, R.; Li, D.; Wagner, S. *Adv. Biomed. Sci. Eng.* **2014**, *1*, 8−18.

(93) Borowiak, R.; Schwaderlapp, N.; Huethe, F.; Lickert, T.; Fischer, E.; Bar, S.; Hennig, J.; von Elverfeldt, D.; Hovener, J.-B. *MAGMA* **2013**, *26* (5), 491−499.
(94) Coffey, A. M.; Shchepin, R. V.; Wilkens, K.; Waddell, K. W.; Chekmenev, E. Y. *J. Magn. Reson.* **2012**, *220*, 94−101.
(95) Kiryutin, A. S.; Sauer, G.; Hadjiali, S.; Yurkovskaya, A. V.; Breitzke, H.; Buntkowsky, G. *J. Magn. Reson.* **2017**, *285*, 26−36.
(96) Hövener, J.-B.; Schwaderlapp, N.; Borowiak, R.; Lickert, T.; Duckett, S. B.; Mewis, R. E.; Adams, R. W.; Burns, M. J.; Highton, L. A. R.; Green, G. G. R.; Olaru, A.; Hennig, J.; von Elverfeldt, D. *Anal. Chem.* **2014**, *86* (3), 1767−1774.
(97) Agraz, J.; Grunfeld, A. M.; Li, D.; Cunningham, K.; Willey, C.; Pozos, R.; Wagner, S. *Rev. Sci. Instrum.* **2014**, *85*, 044705.
(98) Ellermann, F.; Pravdivtsev, A.; Hövener, J.-B. *Magn. Reson.* **2021**, *2* (1), 49−62.
(99) Juarez, A. M.; Cubric, D.; King, G. C. *Meas. Sci. Technol.* **2002**, *13* (5), N52−N55.
(100) Sullivan, N. S.; Zhou, D.; Edwards, C. M. *Cryogenics* **1990**, *30* (8), 734−735.
(101) Hövener, J.-B.; Bär, S.; Leupold, J.; Jenne, K.; Leibfritz, D.; Hennig, J.; Duckett, S. B.; von Elverfeldt, D. *NMR Biomed.* **2013**, *26* (2), 124−131.
(102) Meier, B.; Dumez, J.-N.; Stevanato, G.; Hill-Cousins, J. T.; Roy, S. S.; Håkansson, P.; Mamone, S.; Brown, R. C. D.; Pileio, G.; Levitt, M. H. *J. Am. Chem. Soc.* **2013**, *135* (50), 18746−18749.
(103) Birchall, J. R.; Coffey, A. M.; Goodson, B. M.; Chekmenev, E. Y. *Anal. Chem.* **2020**, *92* (23), 15280−15284.
(104) Sundararajan, K.; Sankaran, K.; Ramanathan, N.; Gopi, R. *J. Mol. Struct.* **2016**, *1117*, 181−191.
(105) Nantogma, S.; Joalland, B.; Wilkens, K.; Chekmenev, E. Y. *Anal. Chem.* **2021**, *93* (7), 3594−3601.
(106) Du, Y.; Zhou, R.; Ferrer, M.-J.; Chen, M.; Graham, J.; Malphurs, B.; Labbe, G.; Huang, W.; Bowers, C. R. *J. Magn. Reson.* **2020**, *321*, 106869.
(107) Buckenmaier, K.; Scheffler, K.; Plaumann, M.; Fehling, P.; Bernarding, J.; Rudolph, M.; Back, C.; Koelle, D.; Kleiner, R.; Hövener, J.; Pravdivtsev, A. N. *ChemPhysChem* **2019**, *20* (21), 2823−2829.
(108) Kiryutin, A. S.; Pravdivtsev, A. N.; Ivanov, K. L.; Grishin, Y. A.; Vieth, H.-M.; Yurkovskaya, A. V. *J. Magn. Reson.* **2016**, *263*, 79−91.
(109) Jeong, K.; Min, S.; Chae, H.; Namgoong, S. K. *Magn. Reson. Chem.* **2018**, *56* (11), 1089−1093.
(110) Gamliel, A.; Allouche-Arnon, H.; Nalbandian, R.; Barzilay, C. M.; Gomori, J. M.; Katz-Brull, R. *Appl. Magn. Reson.* **2010**, *39* (4), 329−345.
(111) Parrott, A. J.; Dallin, P.; Andrews, J.; Richardson, P. M.; Semenova, O.; Halse, M. E.; Duckett, S. B.; Nordon, A. *Appl. Spectrosc.* **2018**, *73* (1), 88−97.
(112) Chapman, B.; Joalland, B.; Meersman, C.; Ettedgui, J.; Swenson, R. E.; Krishna, M. C.; Nikolaou, P.; Kovtunov, K. V.; Salnikov, O. G.; Koptyug, I. V.; Gemeinhardt, M. E.; Goodson, B. M.; Shchepin, R. V.; Chekmenev, E. Y. *Anal. Chem.* **2021**, *93* (24), 8476−8483.
(113) Mhaske, Y.; Sutter, E.; Mahoney, C.; Daley, J.; Whiting, N. 65% Parahydrogen from a Liquid Nitrogen Cooled Generator. In *Parahydrogen Enhanced Resonance Meeting (PERM) 2021*, online, June 21−232021.
(114) Hövener, J.-B.; Pravdivtsev, A. N.; Kidd, B.; Bowers, C. R.; Glöggler, S.; Kovtunov, K. V.; Plaumann, M.; Katz-Brull, R.; Buckenmaier, K.; Jerschow, A.; Reineri, F.; Theis, T.; Shchepin, R. V.; Wagner, S.; Bhattacharya, P.; Zacharias, N. M.; Chekmenev, E. Y. *Angew. Chem., Int. Ed.* **2018**, *57* (35), 11140−11162.
(115) Stewart, N. J.; Nakano, H.; Sugai, S.; Tomohiro, M.; Kase, Y.; Uchio, Y.; Yamaguchi, T.; Matsuo, Y.; Naganuma, T.; Takeda, N.; Nishimura, I.; Hirata, H.; Hashimoto, T.; Matsumoto, S. *ChemPhysChem* **2021**, *22* (10), 915−923.
(116) Sengstschmid, H.; Freeman, R.; Barkemeyer, J.; Bargon, J. *J. Magn. Reson., Ser. A* **1996**, *120* (2), 249−257.
(117) Kiryutin, A. S.; Ivanov, K. L.; Yurkovskaya, A. V.; Vieth, H.-M.; Lukzen, N. N. *Phys. Chem. Chem. Phys.* **2013**, *15* (34), 14248−14255.
(118) Pravdivtsev, A. N.; Sönnichsen, F.; Hövener, J.-B. *J. Magn. Reson.* **2018**, *297*, 86−95.
(119) Pravdivtsev, A. N.; Ivanov, K. L.; Yurkovskaya, A. V.; Vieth, H.-M.; Sagdeev, R. Z. *Dokl. Phys. Chem.* **2015**, *465* (1), 267−269.
(120) Korchak, S.; Emondts, M.; Mamone, S.; Blümich, B.; Glöggler, S. *Phys. Chem. Chem. Phys.* **2019**, *21* (41), 22849−22856.
(121) Sørensen, O. W.; Ernst, R. R. *J. Magn. Reson.* **1983**, *51* (3), 477−489.
(122) Barkemeyer, J.; Bargon, J.; Sengstschmid, H.; Freeman, R. *J. Magn. Reson., Ser. A* **1996**, *120* (1), 129−132.
(123) Pravdivtsev, A. N.; Ellermann, F.; Hövener, J.-B. *Phys. Chem. Chem. Phys.* **2021**, *23* (26), 14146−14150.
(124) Pravdivtsev, A.; Hövener, J.-B.; Schmidt, A. B. Frequency-Selective Manipulations of Spins for Effective and Robust Transfer of Spin Order from Parahydrogen to Heteronuclei in Weakly-Coupled Spin Systems. *ChemPhysChem* DOI: 10.1002/cphc.202100721.
(125) Stewart, N. J.; Kumeta, H.; Tomohiro, M.; Hashimoto, T.; Hatae, N.; Matsumoto, S. *J. Magn. Reson.* **2018**, *296*, 85−92.
(126) Pravdivtsev, A. N.; Yurkovskaya, A. V.; Lukzen, N. N.; Ivanov, K. L.; Vieth, H.-M. *J. Phys. Chem. Lett.* **2014**, *5* (19), 3421−3426.
(127) Rodin, B. A.; Kozinenko, V. P.; Kiryutin, A. S.; Yurkovskaya, A. V.; Eills, J.; Ivanov, K. L. *J. Magn. Reson.* **2021**, *327*, 106978.
(128) Kozinenko, V. P.; Kiryutin, A. S.; Yurkovskaya, A. V.; Ivanov, K. L. *J. Magn. Reson.* **2019**, *309*, 106594.
(129) Korchak, S.; Mamone, S.; Glöggler, S. *ChemistryOpen* **2018**, *7* (9), 672−676.
(130) Svyatova, A.; Kozinenko, V. P.; Chukanov, N. V.; Burueva, D. B.; Chekmenev, E. Y.; Chen, Y.-W.; Hwang, D. W.; Kovtunov, K. V.; Koptyug, I. V. *Sci. Rep.* **2021**, *11* (1), 5646.
(131) Schmidt, A. B. *Liquid-State Nuclear Hyperpolarization without a Polarizer: Synthesis amid the Magnet Bore Allows a Dramatically Enhanced Nuclear Alignment*. Ph.D. Thesis, Albert-Ludwigs-Universität, Freiburg im Breisgau, Germany, 2020.
(132) Korchak, S.; Jagtap, A. P.; Glöggler, S. *Chem. Sci.* **2021**, *12* (1), 314−319.
(133) Lippens, G.; Dhalluin, C.; Wieruszeski, J. M. *J. Biomol. NMR* **1995**, *5* (3), 327−331.
(134) Sklenar, V. *J. Magn. Reson., Ser. A* **1995**, *114* (1), 132−135.
(135) Price, W. S.; Wälchli, M. *Magn. Reson. Chem.* **2002**, *40* (13), S128−S132.
(136) de Maissin, H.; Berner, S.; Ivantaev, V.; Hoevener, J.-B.; Hennig, J.; von Elverfeldt, D.; Schmidt, A. B. Dramatic Effect of Pulse Length and Bandwidth on the Efficiency of Pulsed Spin-Order-Transfer Sequences at High Field. In *Proceedings of the International Socety for Magnetic Resonance in Medicine 29*, online, 2021; 3805
(137) Ivantaev, V.; Berner, S.; de Maissin, H.; Hoevener, J.-B.; Hennig, J.; von Elverfeldt, D.; Kiselev, V.; Schmidt, A. B. Molecular Translation in Inhomogeneous Field Can Dramatically Reduce the Efficiency of Spin-Order Transfer at High Field. In *Proceedings of the International Socety for Magnetic Resonance in Medicine 29*, online, 2021; 3798.
(138) Golman, K.; Olsson, L. E.; Axelsson, O.; Månsson, S.; Karlsson, M.; Petersson, J. S. *Br. J. Radiol.* **2003**, *76* (suppl_2), S118−S127.
(139) Goldman, M.; Jóhannesson, H.; Axelsson, O.; Karlsson, M. *Magn. Reson. Imaging* **2005**, *23* (2), 153−157.
(140) Shchepin, R. V.; Coffey, A. M.; Waddell, K. W.; Chekmenev, E. Y. *J. Phys. Chem. Lett.* **2012**, *3* (22), 3281−3285.
(141) Goodson, B. M.; Whiting, N.; Coffey, A. M.; Nikolaou, P.; Shi, F.; Gust, B. M.; Gemeinhardt, M. E.; Shchepin, R. V.; Skinner, J. G.; Birchall, J. R.; Barlow, M. J.; Chekmenev, E. Y. *eMagRes.* **2015**, *4* (4), 797.
(142) Schmidt, A. B.; Andrews, D. L.; Rohrbach, A.; Gohn-Kreuz, C.; Shatokhin, V. N.; Kiselev, V. G.; Hennig, J.; von Elverfeldt, D.; Hövener, J.-B. *J. Magn. Reson.* **2016**, *268*, 58−67.

(143) Shchepin, R. V.; Coffey, A. M.; Waddell, K. W.; Chekmenev, E. Y. *J. Am. Chem. Soc.* **2012**, *134* (9), 3957−3960.
(144) Bhattacharya, P.; Chekmenev, E. Y.; Perman, W. H.; Harris, K. C.; Lin, A. P.; Norton, V. A.; Tan, C. T.; Ross, B. D.; Weitekamp, D. P. *J. Magn. Reson.* **2007**, *186* (1), 150−155.
(145) Bhattacharya, P.; Chekmenev, E. Y.; Reynolds, W. F.; Wagner, S.; Zacharias, N.; Chan, H. R.; Bünger, R.; Ross, B. D. *NMR Biomed.* **2011**, *24* (8), 1023−1028.
(146) Perman, W. H.; Bhattacharya, P.; Leupold, J.; Lin, A. P.; Harris, K. C.; Norton, V. A.; Hövener, J.-B.; Ross, B. D. *Magn. Reson. Imaging* **2010**, *28* (4), 459−465.
(147) Zacharias, N. M.; Chan, H. R.; Sailasuta, N.; Ross, B. D.; Bhattacharya, P. *J. Am. Chem. Soc.* **2012**, *134* (2), 934−943.
(148) Zacharias, N. M.; McCullough, C. R.; Wagner, S.; Sailasuta, N.; Chan, H. R.; Lee, Y.; Hu, J.; Perman, W. H.; Henneberg, C.; Ross, B. D.; Bhattacharya, P. *J. Mol. Imag. Dyn.* **2016**, *6*, 1000123.
(149) Coffey, A. M.; Feldman, M. A.; Shchepin, R. V.; Barskiy, D. A.; Truong, M. L.; Pham, W.; Chekmenev, E. Y. *J. Magn. Reson.* **2017**, *281* (Supplement C), 246−252.
(150) Salnikov, O. G.; Shchepin, R. V.; Chukanov, N. V.; Jaigirdar, L.; Pham, W.; Kovtunov, K. V.; Koptyug, I. V.; Chekmenev, E. Y. *J. Phys. Chem. C* **2018**, *122* (43), 24740−24749.
(151) Chekmenev, E. Y.; Hövener, J.; Norton, V. A.; Harris, K.; Batchelder, L. S.; Bhattacharya, P.; Ross, B. D.; Weitekamp, D. P. *J. Am. Chem. Soc.* **2008**, *130* (13), 4212−4213.
(152) Olsson, L. E.; Chai, C.-M.; Axelsson, O.; Karlsson, M.; Golman, K.; Petersson, J. S. *Magn. Reson. Med.* **2006**, *55* (4), 731−737.
(153) Reineri, F.; Cavallari, E.; Carrera, C.; Aime, S. *MAGMA* **2021**, *34* (1), 25−47.
(154) Butler, M. C.; Kervern, G.; Theis, T.; Ledbetter, M. P.; Ganssle, P. J.; Blanchard, J. W.; Budker, D.; Pines, A. *J. Chem. Phys.* **2013**, *138* (23), 234201.
(155) Theis, T.; Ganssle, P.; Kervern, G.; Knappe, S.; Kitching, J.; Ledbetter, M. P.; Budker, D.; Pines, A. *Nat. Phys.* **2011**, *7* (7), 571−575.
(156) Emondts, M.; Colell, J. F. P.; Blumich, B.; Schleker, P. P. M. *Phys. Chem. Chem. Phys.* **2017**, *19* (33), 21933−21937.
(157) Pravdivtsev, A. N.; Ivanov, K. L.; Yurkovskaya, A. V.; Vieth, H.-M.; Sagdeev, R. Z. *Dokl. Phys. Chem.* **2015**, *464* (2), 247−250.
(158) Eills, J.; Blanchard, J. W.; Wu, T.; Bengs, C.; Hollenbach, J.; Budker, D.; Levitt, M. H. *J. Chem. Phys.* **2019**, *150* (17), 174202.
(159) Cavallari, E.; Carrera, C.; Aime, S.; Reineri, F. *J. Magn. Reson.* **2018**, *289*, 12−17.
(160) Kuhn, L. T.; Bommerich, U.; Bargon, J. *J. Phys. Chem. A* **2006**, *110* (10), 3521−3526.
(161) Stephan, M.; Kohlmann, O.; Niessen, H. G.; Eichhorn, A.; Bargon, J. *Magn. Reson. Chem.* **2002**, *40* (2), 157−160.
(162) Jonischkeit, T.; Bommerich, U.; Stadler, J.; Woelk, K.; Niessen, H. G.; Bargon, J. *J. Chem. Phys.* **2006**, *124* (20), 201109.
(163) Theis, T.; Truong, M. L.; Coffey, A. M.; Shchepin, R. V.; Waddell, K. W.; Shi, F.; Goodson, B. M.; Warren, W. S.; Chekmenev, E. Y. *J. Am. Chem. Soc.* **2015**, *137* (4), 1404−1407.
(164) Truong, M. L.; Theis, T.; Coffey, A. M.; Shchepin, R. V.; Waddell, K. W.; Shi, F.; Goodson, B. M.; Warren, W. S.; Chekmenev, E. Y. *J. Phys. Chem. C* **2015**, *119* (16), 8786−8797.
(165) Pravdivtsev, A. N.; Ivanov, K. L.; Yurkovskaya, A. V.; Petrov, P. A.; Limbach, H.-H.; Kaptein, R.; Vieth, H.-M. *J. Magn. Reson.* **2015**, *261*, 73−82.
(166) Zhivonitko, V. V.; Skovpin, I. V.; Koptyug, I. V. *Chem. Commun.* **2015**, *51* (13), 2506−2509.
(167) Lindale, J. R.; Eriksson, S. L.; Tanner, C. P. N.; Zhou, Z.; Colell, J. F. P.; Zhang, G.; Bae, J.; Chekmenev, E. Y.; Theis, T.; Warren, W. S. *Nat. Commun.* **2019**, *10* (1), 395.
(168) Pravdivtsev, A. N.; Kempf, N.; Plaumann, M.; Bernarding, J.; Scheffler, K.; Hövener, J.-B.; Buckenmaier, K. *ChemPhysChem* **2021**, DOI: 10.1002/cphc.202100543.
(169) Dagys, L.; Bengs, C.; Levitt, M. H. *J. Chem. Phys.* **2021**, *155* (15), 154201.
(170) Buckenmaier, K.; Rudolph, M.; Fehling, P.; Steffen, T.; Back, C.; Bernard, R.; Pohmann, R.; Bernarding, J.; Kleiner, R.; Koelle, D.; Plaumann, M.; Scheffler, K. *Rev. Sci. Instrum.* **2018**, *89* (12), 125103.
(171) Blanchard, J. W.; Ripka, B.; Suslick, B. A.; Gelevski, D.; Wu, T.; Münnemann, K.; Barskiy, D. A.; Budker, D. *Magn. Reson. Chem.* **2021**, *59*, 1208.
(172) Arunkumar, N.; Bucher, D. B.; Turner, M. J.; TomHon, P.; Glenn, D.; Lehmkuhl, S.; Lukin, M. D.; Park, H.; Rosen, M. S.; Theis, T.; Walsworth, R. L. *PRX Quantum* **2021**, *2* (1), 010305.
(173) Blanchard, J. W.; Ledbetter, M. P.; Theis, T.; Butler, M. C.; Budker, D.; Pines, A. *J. Am. Chem. Soc.* **2013**, *135* (9), 3607−3612.
(174) Blanchard, J. W.; Wu, T.; Eills, J.; Hu, Y.; Budker, D. *J. Magn. Reson.* **2020**, *314*, 106723.
(175) Burueva, D. B.; Eills, J.; Blanchard, J. W.; Garcon, A.; Picazo-Frutos, R.; Kovtunov, K. V.; Koptyug, I. V.; Budker, D. *Angew. Chem., Int. Ed.* **2020**, *59* (39), 17026−17032.
(176) Tayler, M. C. D.; Theis, T.; Sjolander, T. F.; Blanchard, J. W.; Kentner, A.; Pustelny, S.; Pines, A.; Budker, D. *Rev. Sci. Instrum.* **2017**, *88* (9), 091101.
(177) Myers, W.; Slichter, D.; Hatridge, M.; Busch, S.; Mößle, M.; McDermott, R.; Trabesinger, A.; Clarke, J. *J. Magn. Reson.* **2007**, *186* (2), 182−192.
(178) Theis, T.; Blanchard, J. W.; Butler, M. C.; Ledbetter, M. P.; Budker, D.; Pines, A. *Chem. Phys. Lett.* **2013**, *580*, 160−165.
(179) Theis, T.; Ledbetter, M. P.; Kervern, G.; Blanchard, J. W.; Ganssle, P. J.; Butler, M. C.; Shin, H. D.; Budker, D.; Pines, A. *J. Am. Chem. Soc.* **2012**, *134* (9), 3987−3990.
(180) Lee, S.-J.; Jeong, K.; Shim, J. H.; Lee, H. J.; Min, S.; Chae, H.; Namgoong, S. K.; Kim, K. *Sci. Rep.* **2019**, *9* (1), 12422.
(181) Vesanen, P. T.; Nieminen, J. O.; Zevenhoven, K. C. J.; Dabek, J.; Parkkonen, L. T.; Zhdanov, A. V.; Luomahaara, J.; Hassel, J.; Penttilä, J.; Simola, J.; Ahonen, A. I.; Mäkelä, J. P.; Ilmoniemi, R. J. *Magn. Reson. Med.* **2013**, *69* (6), 1795−1804.
(182) Bucher, D. B.; Glenn, D. R.; Park, H.; Lukin, M. D.; Walsworth, R. L. *Phys. Rev. X* **2020**, *10* (2), 021053.
(183) Zheng, H.; Xu, J.; Iwata, G. Z.; Lenz, T.; Michl, J.; Yavkin, B.; Nakamura, K.; Sumiya, H.; Ohshima, T.; Isoya, J.; Wrachtrup, J.; Wickenbrock, A.; Budker, D. *Phys. Rev. Appl.* **2019**, *11* (6), 064068.
(184) Kimmich, R. *Chapter 1 Principle, Purpose and Pitfalls of Field-Cycling NMR Relaxometry*. **2018**, 1−41.
(185) Ivanov, K. L.; Pravdivtsev, A. N.; Yurkovskaya, A. V.; Vieth, H.-M.; Kaptein, R. *Prog. Nucl. Magn. Reson. Spectrosc.* **2014**, *81*, 1−36.
(186) Shchepin, R. V.; Barskiy, D. A.; Coffey, A. M.; Manzanera Esteve, I. V.; Chekmenev, E. Y. *Angew. Chem., Int. Ed.* **2016**, *55* (20), 6071−6074.
(187) Reineri, F.; Viale, A.; Dastrù, W.; Gobetto, R.; Aime, S. *Contrast Media Mol. Imaging* **2011**, *6* (2), 77−84.
(188) Reineri, F.; Viale, A.; Ellena, S.; Alberti, D.; Boi, T.; Giovenzana, G. B.; Gobetto, R.; Premkumar, S. S. D.; Aime, S. *J. Am. Chem. Soc.* **2012**, *134* (27), 11146−11152.
(189) Ellena, S.; Viale, A.; Gobetto, R.; Aime, S. *Magn. Reson. Chem.* **2012**, *50* (8), 529−533.
(190) Eills, J.; Cavallari, E.; Carrera, C.; Budker, D.; Aime, S.; Reineri, F. *J. Am. Chem. Soc.* **2019**, *141* (51), 20209−20214.
(191) Ripka, B.; Eills, J.; Kourilova, H.; Leutzsch, M.; Levitt, M. H.; Munnemann, K. *Chem. Commun.* **2018**, *54* (86), 12246−12249.
(192) Rodin, B. A.; Eills, J.; Picazo-Frutos, R.; Sheberstov, K. F.; Budker, D.; Ivanov, K. L. *Phys. Chem. Chem. Phys.* **2021**, *23* (12), 7125−7134.
(193) Reineri, F.; Santelia, D.; Gobetto, R.; Aime, S. *J. Magn. Reson.* **2009**, *200* (1), 15−20.
(194) Pokochueva, E. V.; Burueva, D. B.; Salnikov, O. G.; Koptyug, I. V. *ChemPhysChem* **2021**, *22* (14), 1421−1440.
(195) Kovtunov, K. V.; Barskiy, D. A.; Shchepin, R. V.; Coffey, A. M.; Waddell, K. W.; Koptyug, I. V.; Chekmenev, E. Y. *Anal. Chem.* **2014**, *86* (13), 6192−6196.
(196) Kovtunov, K. V.; Zhivonitko, V. V.; Skovpin, I. V.; Barskiy, D. A.; Salnikov, O. G.; Koptyug, I. V. *J. Phys. Chem. C* **2013**, *117* (44), 22887−22893.

(197) Salnikov, O. G.; Kovtunov, K. V.; Koptyug, I. V. *Sci. Rep.* **2015**, *5* (1), 13930.
(198) Salnikov, O. G.; Svyatova, A.; Kovtunova, L. M.; Chukanov, N. V.; Bukhtiyarov, V. I.; Kovtunov, K. V.; Chekmenev, E. Y.; Koptyug, I. V. *Chem. - Eur. J.* **2021**, *27* (4), 1316−1322.
(199) Du, Y.; Behera, R.; Maligal-Ganesh, R. V.; Chen, M.; Chekmenev, E. Y.; Huang, W.; Bowers, C. R. *J. Phys. Chem. C* **2020**, *124* (15), 8304−8309.
(200) Zhou, R.; Cheng, W.; Neal, L. M.; Zhao, E. W.; Ludden, K.; Hagelin-Weaver, H. E.; Bowers, C. R. *Phys. Chem. Chem. Phys.* **2015**, *17* (39), 26121−26129.
(201) Burueva, D. B.; Kozinenko, V. P.; Sviyazov, S. V.; Kovtunova, L. M.; Bukhtiyarov, V. I.; Chekmenev, E. Y.; Salnikov, O. G.; Kovtunov, K. V.; Koptyug, I. V. *Appl. Magn. Reson.* **2021**, DOI: 10.1007/s00723-021-01377-4.
(202) Salnikov, O. G.; Nikolaou, P.; Ariyasingha, N. M.; Kovtunov, K. V.; Koptyug, I. V.; Chekmenev, E. Y. *Anal. Chem.* **2019**, *91* (7), 4741−4746.
(203) Kovtunov, K. V.; Barskiy, D. A.; Coffey, A. M.; Truong, M. L.; Salnikov, O. G.; Khudorozhkov, A. K.; Inozemtseva, E. A.; Prosvirin, I. P.; Bukhtiyarov, V. I.; Waddell, K. W.; Chekmenev, E. Y.; Koptyug, I. V. *Chem. - Eur. J.* **2014**, *20* (37), 11636−11639.
(204) Salnikov, O. G.; Kovtunov, K. V.; Nikolaou, P.; Kovtunova, L. M.; Bukhtiyarov, V. I.; Koptyug, I. V.; Chekmenev, E. Y. *ChemPhysChem* **2018**, *19* (20), 2621−2626.
(205) Burueva, D. B.; Kovtunov, K. V.; Bukhtiyarov, A. V.; Barskiy, D. A.; Prosvirin, I. P.; Mashkovsky, I. S.; Baeva, G. N.; Bukhtiyarov, V. I.; Stakheev, A. Yu; Koptyug, I. V. *Chem. - Eur. J.* **2018**, *24* (11), 2547−2553.
(206) Telkki, V.-V.; Zhivonitko, V. V.; Ahola, S.; Kovtunov, K. V.; Jokisaari, J.; Koptyug, I. V. *Angew. Chem., Int. Ed.* **2010**, *49* (45), 8363−8366.
(207) Telkki, V.-V.; Zhivonitko, V. V. *J. Magn. Reson.* **2011**, *210* (2), 238−245.
(208) Bouchard, L.-S.; Burt, S. R.; Anwar, M. S.; Kovtunov, K. V.; Koptyug, I. V.; Pines, A. *Science* **2008**, *319* (5862), 442−445.
(209) Zhivonitko, V. V.; Telkki, V.-V.; Koptyug, I. V. *Angew. Chem.* **2012**, *124* (32), 8178−8182.
(210) Kovtunov, K. V.; Lebedev, D.; Svyatova, A.; Pokochueva, E. V.; Prosvirin, I. P.; Gerasimov, E. Y.; Bukhtiyarov, V. I.; Müller, C. R.; Fedorov, A.; Koptyug, I. V. *ChemCatChem* **2018**, *11* (3), 969−973.
(211) Svyatova, A.; Kononenko, E. S.; Kovtunov, K. V.; Lebedev, D.; Gerasimov, E. Y.; Bukhtiyarov, A. V.; Prosvirin, I. P.; Bukhtiyarov, V. I.; Muller, C. R.; Fedorov, A.; Koptyug, I. V. *Catal. Sci. Technol.* **2020**, *10* (1), 99−104.
(212) Barskiy, D. A.; Kovtunov, K. V.; Gerasimov, E. Y.; Phipps, M. A.; Salnikov, O. G.; Coffey, A. M.; Kovtunova, L. M.; Prosvirin, I. P.; Bukhtiyarov, V. I.; Koptyug, I. V.; Chekmenev, E. Y. *J. Phys. Chem. C* **2017**, *121* (18), 10038−10046.
(213) Ariyasingha, N. M.; Salnikov, O. G.; Kovtunov, K. V.; Kovtunova, L. M.; Bukhtiyarov, V. I.; Goodson, B. M.; Rosen, M. S.; Koptyug, I. V.; Gelovani, J. G.; Chekmenev, E. Y. *J. Phys. Chem. C* **2019**, *123* (18), 11734−11744.
(214) Barskiy, D. A.; Salnikov, O. G.; Romanov, A. S.; Feldman, M. A.; Coffey, A. M.; Kovtunov, K. V.; Koptyug, I. V.; Chekmenev, E. Y. *J. Magn. Reson.* **2017**, *276*, 78−85.
(215) Ariyasingha, N. M.; Joalland, B.; Younes, H. R.; Salnikov, O. G.; Chukanov, N. V.; Kovtunov, K. V.; Kovtunova, L. M.; Bukhtiyarov, V. I.; Koptyug, I. V.; Gelovani, J. G.; Chekmenev, E. Y. *Chem. - Eur. J.* **2020**, *26* (60), 13621−13626.
(216) Zhao, E. W.; Maligal-Ganesh, R.; Xiao, C.; Goh, T.-W.; Qi, Z.; Pei, Y.; Hagelin-Weaver, H. E.; Huang, W.; Bowers, C. R. *Angew. Chem.* **2017**, *129* (14), 3983−3987.
(217) Zhao, E. W.; Xin, Y.; Hagelin-Weaver, H. E.; Bowers, C. R. *ChemCatChem* **2016**, *8* (13), 2197−2201.
(218) Barskiy, D. A.; Salnikov, O. G.; Kovtunov, K. V.; Koptyug, I. V. *J. Phys. Chem. A* **2015**, *119* (6), 996−1006.
(219) Sharma, R.; Bouchard, L.-S. *Sci. Rep.* **2012**, *2* (1), 277.
(220) Kidd, B. E.; Gesiorski, J. L.; Gemeinhardt, M. E.; Shchepin, R. V.; Kovtunov, K. V.; Koptyug, I. V.; Chekmenev, E. Y.; Goodson, B. M. *J. Phys. Chem. C* **2018**, *122* (29), 16848−16852.
(221) Cavallari, E.; Carrera, C.; Di Matteo, G.; Bondar, O.; Aime, S.; Reineri, F. *Front. Oncol.* **2020**, *10*, 497.
(222) Bondar, O.; Cavallari, E.; Carrera, C.; Aime, S.; Reineri, F. *arXiv* **2021**, 210801497.
(223) Cavallari, E.; Carrera, C.; Aime, S.; Reineri, F. *ChemPhysChem* **2019**, *20* (2), 318−325.
(224) Cavallari, E.; Carrera, C.; Reineri, F. *Isr. J. Chem.* **2017**, *57* (9), 833−842.
(225) Srour, M.; Hadjiali, S.; Brunnengräber, K.; Weidler, H.; Xu, Y.; Breitzke, H.; Gutmann, T.; Buntkowsky, G. *J. Phys. Chem. C* **2021**, *125* (13), 7178−7187.
(226) Pokochueva, E. V.; Kovtunov, K. V.; Salnikov, O. G.; Gemeinhardt, M. E.; Kovtunova, L. M.; Bukhtiyarov, V. I.; Chekmenev, E. Y.; Goodson, B. M.; Koptyug, I. V. *Phys. Chem. Chem. Phys.* **2019**, *21* (48), 26477−26482.
(227) Salnikov, O. G.; Chukanov, N. V.; Shchepin, R. V.; Manzanera Esteve, I. V.; Kovtunov, K. V.; Koptyug, I. V.; Chekmenev, E. Y. *J. Phys. Chem. C* **2019**, *123* (20), 12827−12840.
(228) McCormick, J.; Grunfeld, A. M.; Ertas, Y. N.; Biswas, A. N.; Marsh, K. L.; Wagner, S.; Glöggler, S.; Bouchard, L.-S. *Anal. Chem.* **2017**, *89* (13), 7190−7194.
(229) Pei, Y.; Chen, M.; Zhong, X.; Zhao, T. Y.; Ferrer, M.-J.; Maligal-Ganesh, R. V.; Ma, T.; Zhang, B.; Qi, Z.; Zhou, L.; Bowers, C. R.; Liu, C.; Huang, W. *Nanoscale* **2020**, *12* (15), 8519−8524.
(230) McCormick, J.; Korchak, S.; Mamone, S.; Ertas, Y.; Liu, Z.; Verlinsky, L.; Wagner, S.; Gloeggler, S.; Bouchard, L. *Angew. Chem., Int. Ed.* **2018**, *57* (33), 10692.
(231) Kadlecek, S.; Shaghaghi, H.; Siddiqui, S.; Profka, H.; Pourfathi, M.; Rizi, R. *NMR Biomed.* **2014**, *27* (12), 1557−1570.
(232) Eills, J.; Alonso-Valdesueiro, J.; Salazar Marcano, D. E.; Ferreira da Silva, J.; Alom, S.; Rees, G. J.; Hanna, J. V.; Carravetta, M.; Levitt, M. H. *ChemPhysChem* **2018**, *19* (1), 40−44.
(233) Eills, J.; Hale, W.; Sharma, M.; Rossetto, M.; Levitt, M. H.; Utz, M. *J. Am. Chem. Soc.* **2019**, *141* (25), 9955−9963.
(234) Bordonali, L.; Nordin, N.; Fuhrer, E.; MacKinnon, N.; Korvink, J. G. *Lab Chip* **2019**, *19* (3), 503−512.
(235) Ostrowska, S. J.; Rana, A.; Utz, M. *ChemPhysChem* **2021**, *22* (19), 2004−2013.
(236) Eills, J.; Hale, W.; Utz, M. *Prog. Nucl. Magn. Reson. Spectrosc.* **2021**, DOI: 10.1016/j.pnmrs.2021.09.001.
(237) Suefke, M.; Lehmkuhl, S.; Liebisch, A.; Blümich, B.; Appelt, S. *Nat. Phys.* **2017**, *13* (6), 568−572.
(238) Joalland, B.; Theis, T.; Appelt, S.; Chekmenev, E. Y. *Angew. Chem., Int. Ed.* **2021**, *60* (50), 26298−26302.
(239) Gilles, H.; Monfort, Y.; Hamel, J. *Rev. Sci. Instrum.* **2003**, *74* (10), 4515−4520.
(240) Heil, W.; Gemmel, C.; Karpuk, S.; Sobolev, Y.; Tullney, K.; Allmendinger, F.; Schmidt, U.; Burghoff, M.; Kilian, W.; Knappe-Grüneberg, S.; Schnabel, A.; Seifert, F.; Trahms, L. *Ann. Phys.* **2013**, *525* (8−9), 539−549.
(241) Chen, H.-Y.; Lee, Y.; Bowen, S.; Hilty, C. *J. Magn. Reson.* **2011**, *208* (2), 204−209.
(242) Iali, W.; Rayner, P. J.; Duckett, S. B. *Sci. Adv.* **2018**, *4* (1), No. eaao6250.
(243) Richardson, P. M.; John, R. O.; Parrott, A. J.; Rayner, P. J.; Iali, W.; Nordon, A.; Halse, M. E.; Duckett, S. B. *Phys. Chem. Chem. Phys.* **2018**, *20* (41), 26362−26371.
(244) Knecht, S.; Barskiy, D. A.; Buntkowsky, G.; Ivanov, K. L. *J. Chem. Phys.* **2020**, *153* (16), 164106.